Supporting Information

Catalytic dehydrocoupling of methylamine borane using Yamashita's [Ir(PBP)] boryl complex - characterisation of a novel highly fluxional Ir tetrahydride

David Decker[1], Hans-Joachim Drexler[1], Wolfgang Baumann[1], Fabian Reiß[1], Torsten Beweries[1]

[1]Leibniz-Institut für Katalyse e.V. (LIKAT), Albert-Einstein-Str. 29a, 18059 Rostock, Germany.

Table of Contents

1 Experimental Section

General Information

All experiments, unless otherwise stated, were performed under oxygen- and moisture-free conditions under an inert atmosphere of argon using standard Schlenk or glove box techniques. All glassware was heated three times *in vacuo* using a heat gun and cooled under argon atmosphere. Solvents and reactants were either obtained from commercial sources (table 1.) THF, dichloromethane,toluene, *n*-hexane, *n*-pentane, diethylether and benzene were dispensed from a solvent purification system (SPS) (PureSolv, Innovative Technology) into thick-walled glass Schlenk bombs equipped with Young-type Teflon valve stopcocks, cannula transferred onto activated molecular sieves (3 Å, 0.3 nm, Carl Roth) and stored under argon in a conventional Schlenk flask. Complex $^{t\text{Bu}}$PBPIr(H)Cl (**1**) was synthesised following literature procedures.[1]

Table S 1. Origin and purification of solvents and reactants.

Substance	Origin	Purification
CH_2Cl_2	local trade	taken from SPS and stored over molecular sieves (3 Å)
THF	local trade	taken from SPS and stored over molecular sieves (3 Å)
benzene	local trade	dried over Na/benzophenone stored over molecular sieves (3 Å)
toluene	local trade	taken from SPS and stored over molecular sieves (3 Å)
n-pentane	local trade	dried over Na/benzophenone stored over molecular sieves (3 Å)
n-hexane	local trade	taken from SPS and stored over molecular sieves (3 Å)
CD_2Cl_2	euriso-top	dried over molecular sieves (3 Å), degassed (three freeze-pump-thaw cycles) and stored in glove box
$CDCl_3$	euriso-top	dried over molecular sieves (3 Å), degassed (three freeze-pump-thaw cycles) and stored in glove box
C_6D_6	euriso-top	dried over molecular sieves (3 Å), degassed (three freeze-pump-thaw cycles) and stored in glove box
toluene-d_8	euriso-top	dried over molecular sieves (3 Å), degassed (three freeze-pump-thaw cycles) and stored in glove box
$[Ir(COD)Cl]_2$	sigma aldrich	

NMR spectra

^{1}H, $^{1}H\{^{31}P\}$ ^{11}B, $^{11}B\{^{1}H\}$, $^{13}C\{^{1}H\}$ and $^{31}P\{^{1}H\}$ NMR spectra were recorded at room temperature on Bruker AV300, AV400 or Fourier300 spectrometers. All ^{1}H and ^{13}C chemical shifts were referenced to the solvent signal. (CD_2Cl_2: δ_H = 5.32 ppm, δ_C = 53.84 ppm, $CDCl_3$: δ_H = 7.26 ppm, δ_C = 77.16 ppm, C_6D_6: δ_H = 7.16 ppm, δ_C = 128.06 ppm, toluene-d_8: δ_H = 7.09 ppm, δ_C = 137.48 ppm, DMSO-d_6: δ_H = 2.50 ppm, δ_C = 39.52 ppm).

IR spectra of crystalline samples were recorded on a Bruker Alpha II FT-IR spectrometer equipped with an ATR unit at ambient temperature under argon atmosphere or on a Bruker Alpha FT-IR-spectrometer equipped with an ATR unit at ambient temperature under aerobic conditions.

Elemental analyses were obtained using a Leco TruSpec Micro CHNS analyser. V_2O_5 was used as an oxidiser for CHN analysis of Ir complexes, circumventing possible Ir carbide formation.

Melting points (uncorrected) were determined using a Mettler-Toledo MP 70 Melt at a heating rate of 5 °C/min. Clearing points are reported.

Mass spectra were recorded on a Thermo Electron MAT 95-XP sector field mass spectrometer using crystalline samples.

UV/vis spectra were recorded on a SPECORD S 600 UV/VIS spectrometer with a diode-array detector. The samples were dissolved in toluene in a 1 cm quartz cuvette with a Schlenk-Valve.

SEC analysis was done using a 1100 GPC (Agilent Technologies) with a refraction index detector at 25 °C. The measurements were performed at a constant temperature of 25 °C using three columns with a polyester copolymer network as stationary phase (PSS GRAM 1000 Å, 5 µm particle size, 8.0 × 300 mm; PSS GRAM 100 000 Å, 5 µm particle size, 8.0 × 300 mm; PSS GRAM 1 000 000 Å). Non-stabilised THF (HPLC grade) with 1 w% Bu_4NBr added was applied as the mobile phase with a flow rate of 1 mL min^{-1}. For this purpose, 1−3 mg of the sample were dissolved in 1 mL of THF. For the recording and the evaluation of the measurement the software PSS WINGPC 6®UniChrome (PSS) was used.

2 Crystallographic Details

X-ray Structure Determination

X-ray quality crystals were selected in Fomblin YR-1800 perfluoroether (Alfa Aesar) at low temperature. Diffraction data were collected at 123(2) K on a Bruker Kappa APEX II Duo diffractometer using Mo-K_α radiation **2** or Cu-K_α radiation **4**. The structures were solved by iterative (SHELXT)[2] or direct methods (SHELXS-97)[3] and refined by full matrix least square techniques against F^2 (SHELXL-2014)[4]. Semi-empirical absorption corrections were applied (SADABS[5] or TWINABS[6]/Bruker). The non-hydrogen atoms were refined anisotropically. The hydrogen atoms, except the hydrides, were placed into theoretical positions and were refined using the riding model. DIAMOND (Crystal Impact GbR) was used for structure representations.

For complex **4**, electron densities up to 2.2 e/Å^3 are found at a distance of about 0.8 Å from the Ir centre. Therefore, in the last refinement cycles, the positions of H2Ir and H4Ir had to be fixed with restraints.

Crystallographic data (excluding structure factors) for the structures reported in this paper have been deposited at the Cambridge Crystallographic Data Centre. Copies of the data can be obtained free of charge on application to CCDC, 12 Union Road, Cambridge, CB21EZ, UK (fax: int. code + (1223) 336-033; e-mail: deposit@ccdc.cam.ac.uk

Table S 2. Crystallographic details.

Compound	[($^{t\text{Bu}}$PBP)Ir(H)$_2$(CO)] (**2**)	[($^{t\text{Bu}}$PBP)Ir(H)$_4$] (**4**)
Chem. Formula	$C_{25}H_{46}BIrN_2OP_2$, C_4H_8O	$C_{24}H_{48}BIrN_2P_2$, C_7H_8
Formula weight [g/mol]	727.69	721.72
Colour	red	colourless
Crystal system	orthorhombic	monoclinic
Space group	*P*bca	$P2_1/c$
a [Å]	15.5170(6)	19.1126(7)
b [Å]	12.1309(5)	15.5043(6)
c [Å]	34.2767(13)	11.6052(4)
α [°]	90	90
β [°]	90	106.885(2)
γ [°]	90	90
V [Å^3]	6452.1(44)	3290.7(2)
Z	8	4
$\rho_{calcd.}$ [g/cm^3]	1.498	1.457
μ [mm^{-1}]	4.265	8.919
T [K]	150(2)	150(2)
Measured reflections	103504	5445
Independent reflections	6333	5445
Reflections with $I > 2\sigma(I)$	5497	4370
R_{int}	0.0437	0.0855
F(000)	2960	1472
$R_1(R[F^2>2\sigma(F^2)])$	0.0222	0.0614
w$R_2(F^2)$	0.0483	0.1519
GooF	1.078	1.079
No. of Parameters	354	363
CCDC #	2204735	2204734

3 Preparation of complexes

3.1 Synthesis of [(^{tBu}PBP)Ir(H)$_2$(CO)] (2)

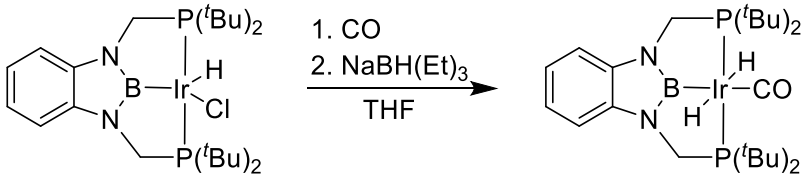

1 **2**

Complex **1** (132 mg, 199 µmol) was dissolved in THF (8 mL) at room temperature. The reaction mixture was degassed (one freeze-pump-thaw-cycle) and CO gas (1 atm) was added to the reaction mixture at room temperature for 30 min. During that, a colour change from yellow to bright yellow was observed. The reaction mixture was cooled to −78 °C, cold $NaBEt_3H$ (219 µL, 219 µmol, 1.0 mol·L^{-1} in toluene) was slowly added and the mixture was stirred for another 15 min at ambient temperature. The reaction mixture was warmed to room temperature and stirred for another 10 min at this temperature. The solvent was removed in vacuum and the residue was extracted with benzene (2x5 mL). The solvent of the extract was removed in vacuum, yielding an orange/red coloured amorphous solid, which was recrystallised from a saturated benzene solution at room temperature to yield orange crystals (75.6 mg, 115 µmol, 58%).

^{1}H NMR (400 MHz, CD_2Cl_2): δ −12.23 (t, J = 14.6 Hz, 2H, 2x Ir-*H*), 1.36 (t, J = 6.7 Hz, 36H, 2x PC(C*H*$_3$)$_3$), 3.82 (t, J = 2.3 Hz, 4H, 2x C*H*$_2$), 6.72−6.81 (m, 4H, Ar-*H*) ppm. **^{31}P{^{1}H} NMR** (162 MHz, CD_2Cl_2): δ 88.6 (s) ppm. **^{11}B{^{1}H} NMR** (96 MHz, toluene-d_8): δ 52.7 (br s) ppm. **^{13}C{^{1}H} NMR** (101 MHz, toluene-d_8): 29.7 (PC(*C*H$_3$)$_3$), 34.9 (P*C*(CH$_3$)$_3$), 43.5 (*C*H$_2$), 108.7 (*m*-*C*$_{Ar}$), 118.0 (*o*-*C*$_{Ar}$), 140.8(*C*$_{q\text{-}Ar}$), 183.0 (*C*O) ppm. **IR** (ATR, 32 scans, cm^{-1}): $\tilde{\nu}$ 2037.0 cm^{-1} (Ir−H), 1963.6 cm^{-1} (Ir−CO), 1818.8 cm^{-1} (Ir−H). **MS** (CI+, *iso*-butane) *m*/*z* (%): 654 [M-H$^+$], 655 [M-H$^+$].

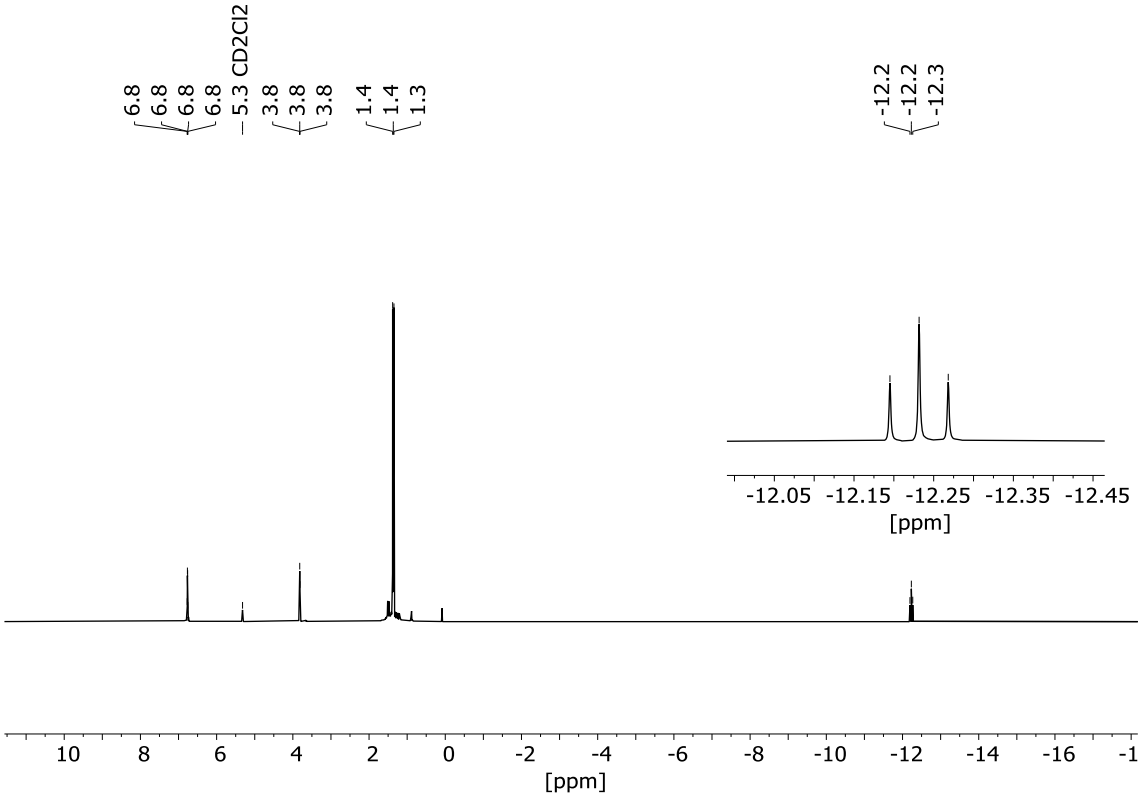

Figure S 1. ^{1}H NMR spectrum (CD_2Cl_2, 400 MHz, 298 K) of complex **2**.

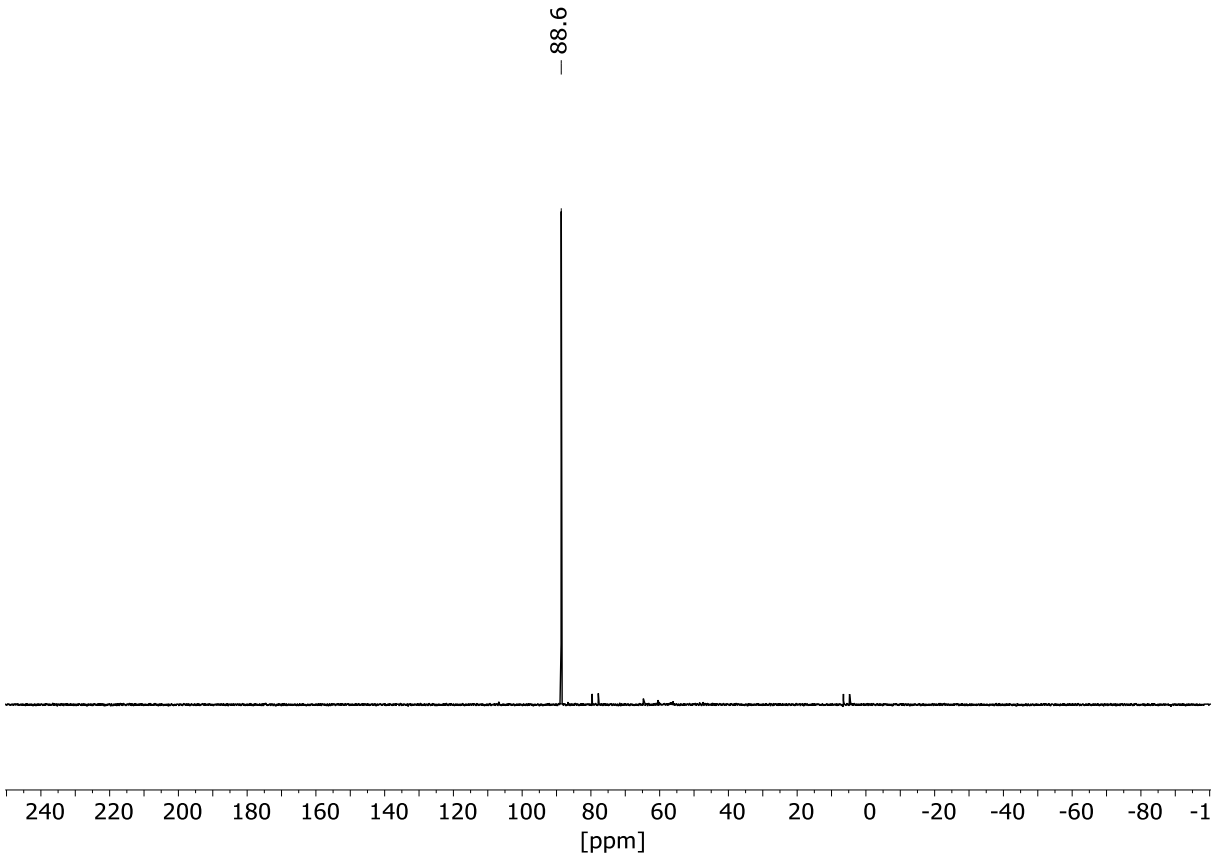

Figure S 2. $^{31}P\{^{1}H\}$ NMR spectrum (CD_2Cl_2, 162 MHz, 298 K) of complex **2**.

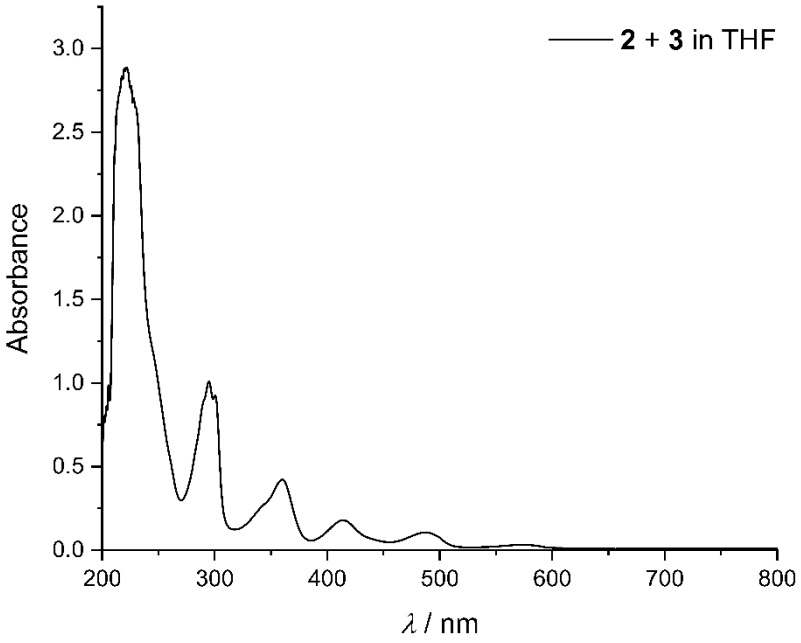

Figure S 3. UV/vis spectrum of complex **2**+**3** in THF.

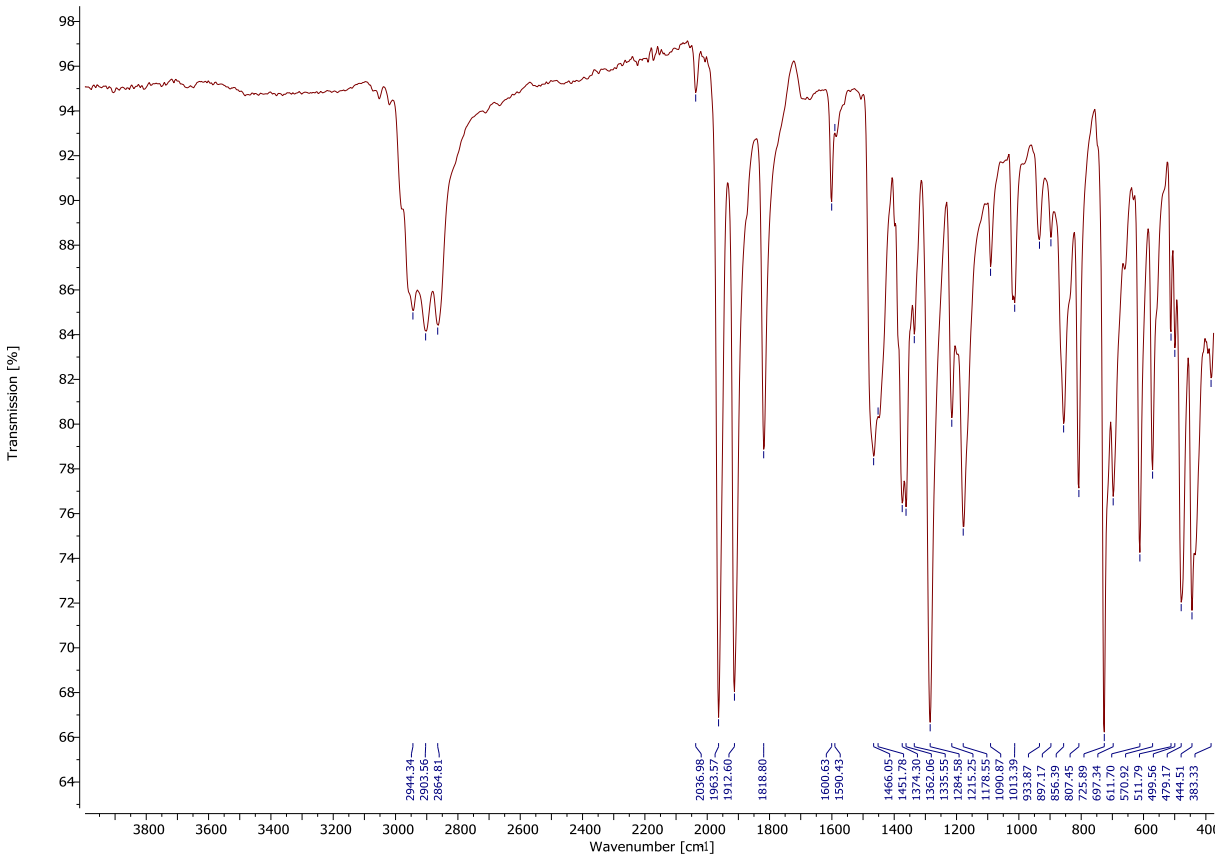

Figure S 4. IR spectrum of complex **2**.

3.2 Synthesis of [(^{tBu}PBP)Ir(CO)] (3)

Complex **1** (135 mg, 204 µmol) was dissolved in toluene (8 mL) at room temperature. The reaction mixture was degassed (one freeze-pump-thaw-cycle) and CO gas (1 atm) was added to the reaction mixture at room temperature for 30 min. During that, a colour change from yellow to bright yellow was observed. The reaction mixture was cooled to −78 °C, cold Na-BEt_3H (224 µL, 224 µmol, 1.0 mol·L^{-1} in toluene) was slowly added and the mixture was stirred for another 15 min at ambient temperature. The reaction mixture was warmed to room temperature and stirred for another 10 min at this temperature. The solvent was removed in vacuum and the residue was extracted with pentane (2x5 mL). The solvent of the extract was removed in vacuum, yielding a red coloured amorphous solid, which was recrystallised from a saturated benzene solution at room temperature to yield red crystals (68.1 mg, 104.2 µmol, 51%).

^{1}H NMR (300 MHz, C_6D_6): δ 1.24 (t, J = 6.6 Hz, 36 H, 2x PC(CH_3)$_3$), 3.99 (s, 4H, 2x CH_2), 7.03−7.08 (m, 2H, Ar-*H*), 7.15−7.18 (m, 2H, Ar-*H*) ppm. **^{31}P{^{1}H} NMR** (122 MHz, C_6D_6): δ 107.2 (s) ppm. **^{11}B{^{1}H} NMR** (96 MHz, C_6D_6): δ 61.8 (br s) ppm. **^{13}C{^{1}H} NMR** (75 MHz, C_6D_6): δ 29.9 (t, J = 3.1 Hz, PC(CH_3)$_3$), 37.1 (t, J = 9.2 Hz, PC(CH_3)$_3$), 43.6 (t, J = 19.8 Hz CH_2), 109.8 (s, *m*-C_{Ar}), 118.7 (s, *o*-C_{Ar}), 139.9 140.8(s, $C_{q\text{-}Ar}$), 211.4 (s, CO) ppm. **IR** (ATR, 32 scans, cm^{-1}): $\tilde{\nu}$ 1912.6 cm^{-1} (Ir−CO). **MS** (CI+, *iso*-butane) *m*/*z* (%): 655 [M+H$^+$].

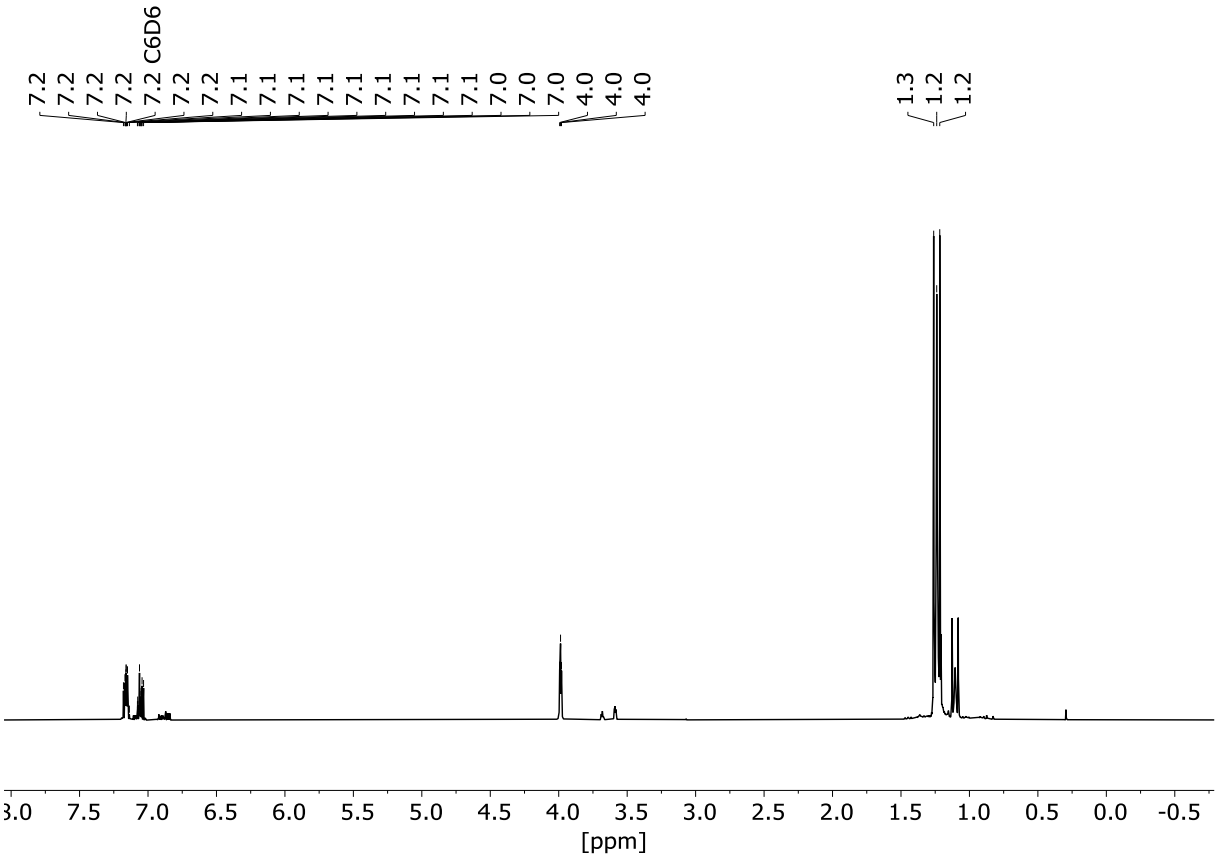

Figure S 5. ^{1}H NMR spectrum (C_6D_6, 300 MHz, 298 K) of complex **3**.

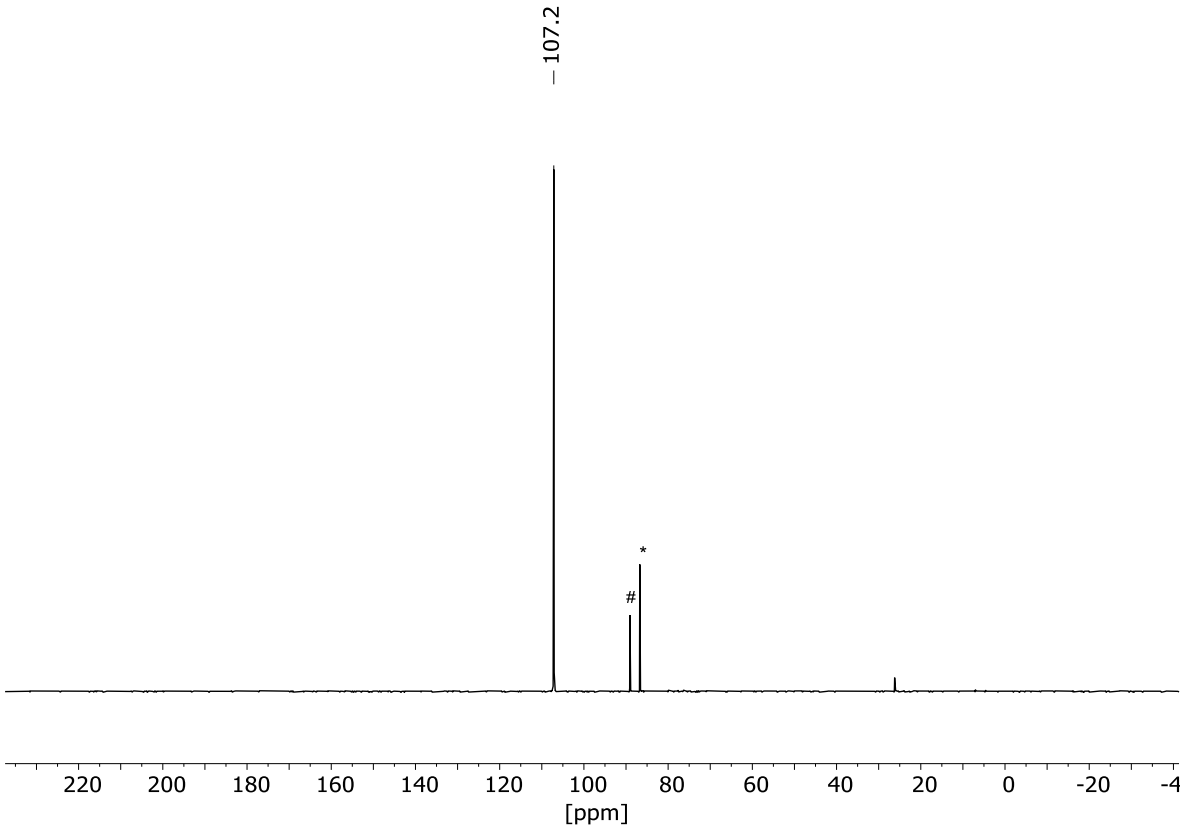

Figure S 6. $^{31}P\{^{1}H\}$ NMR spectrum (C_6D_6, 122 MHz, 298 K) of complex **3**. * complex **1**, # complex **2**.

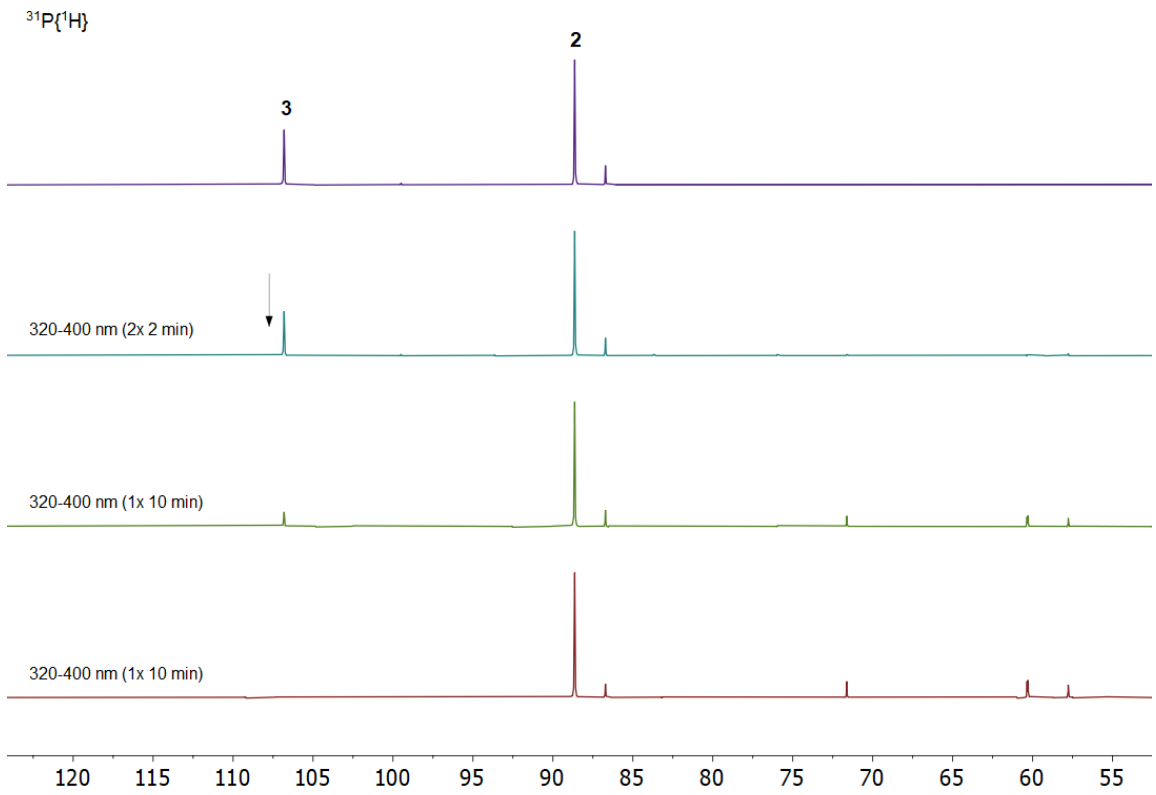

Figure S 7. $^{31}P\{^{1}H\}$ NMR spectrum (CD_2Cl_2, 122 MHz, 298 K) of a mixture of complexes **2** and **3**. Top: before irradiation (λ = 320−400 nm). Bottom: after irradiation (t_{total} = 24 min). Photodissociation of CO from **3** was observed.

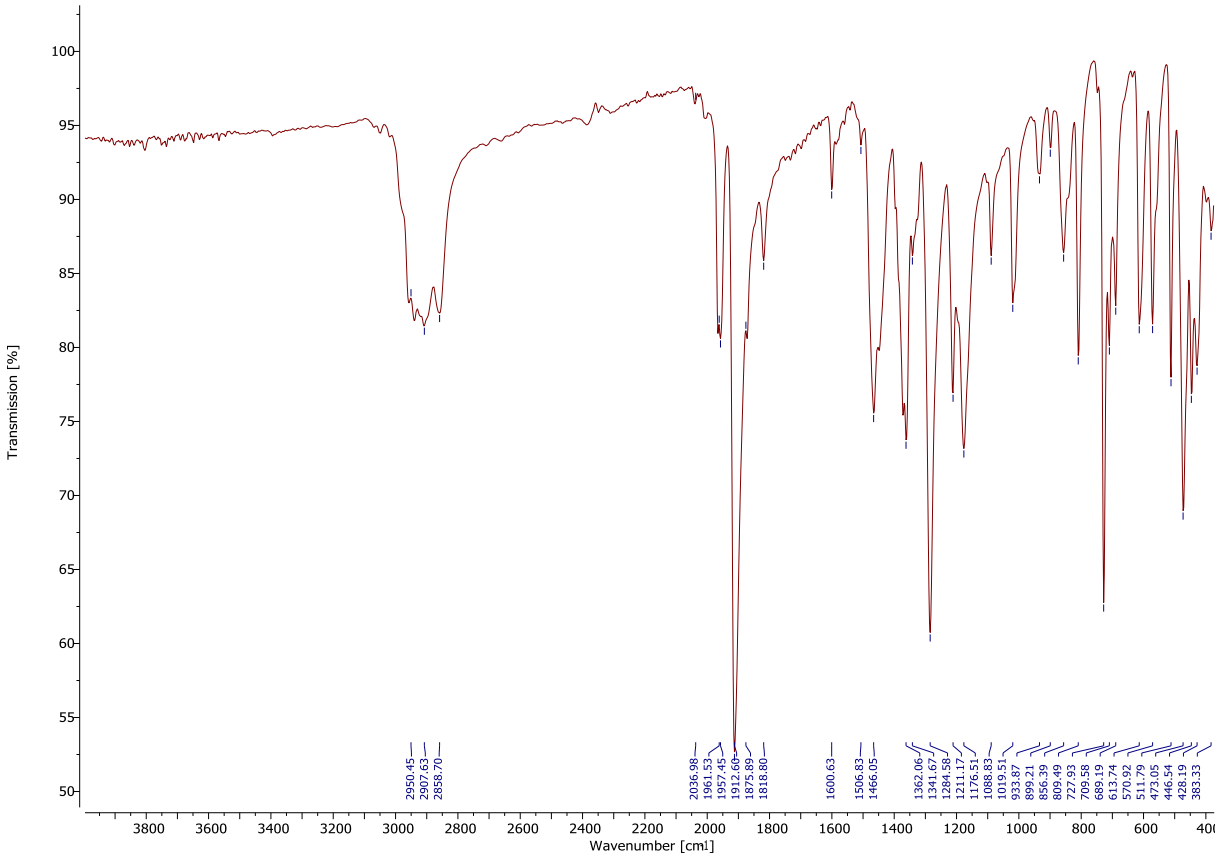

Figure S 8. IR spectrum of complex **3**.

3.3 Stoichiometric reaction of complex 1 with $H_3B{\cdot}NMeH_2$

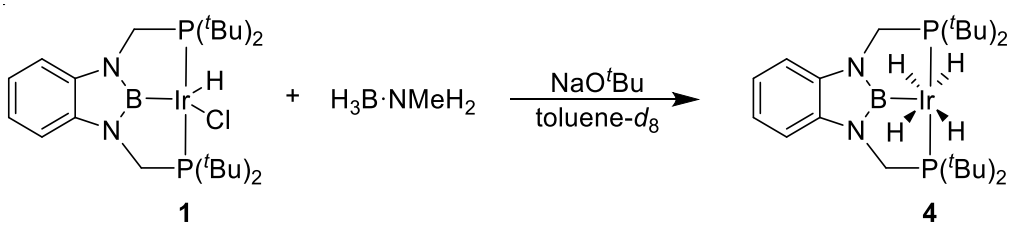

1 **4**

Precatalyst **1** (23.0 mg, 34.7 µmol), $H_3B{\cdot}NMeH_2$ (1.56 mg, 34.7 µmol) and NaO*t*Bu (3.51 mg, 36.5 µmol) were dissolved in toluene-d_8 (0.7 mL) in a Young-NMR-tube. The colour of the reaction mixture turns from yellow to dark brown within a few minutes. ^{1}H NMR monitoring of the progress of the reaction shows a broad singlet at −10.0 ppm. The reaction mixture was filtered under hydrogen atmosphere. The solvent was evaporated in a hydrogen stream to ≈ 0.2 mL. After few days colourless crystals of **4** were formed and analysed by X-ray diffraction. Removing the solvent in vacuo, results in the formation of undefined reaction products.

^{1}H NMR (400 MHz, C_6D_6): δ −9.88 (br. s, 4 H), 1.19 (t, J = 6.8 Hz, 36 H, 2x PC(C*H*$_3$)$_3$), 3.56 (t, J = 2.3 Hz 4 H, 2x C*H*$_2$), 6.86−6.94 (m, 2H, Ar-*H*), 7.04−7.11 (m, 2H, Ar-*H*) ppm. **^{31}P{^{1}H} NMR** (162 MHz, C_6D_6): δ 87.7 (s) ppm. **^{11}B NMR** (128 MHz, C_6D_6): δ 50.5 (br s) ppm. **^{13}C{^{1}H} NMR** (101 MHz, C_6D_6): δ 29.5 (PC(*C*H$_3$)$_3$), 33.3 (P*C*(CH$_3$)$_3$), 43.1 (*C*H$_2$), 108.5 (*m*-*C*$_{Ar}$), 118.2 (*o*-*C*$_{Ar}$), 142.2 (*C*$_{q\text{-}Ar}$) ppm.

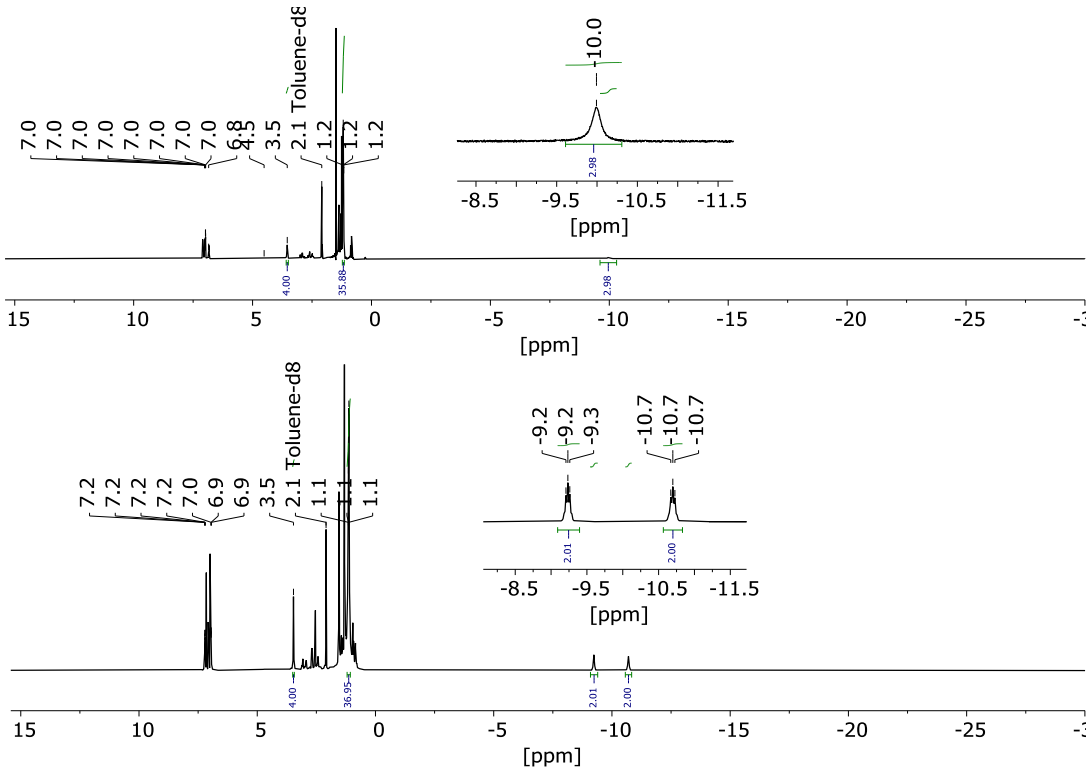

Figure S 9. Top: *in situ* ^{1}H NMR spectrum (toluene-d_8, 300 MHz) of the reaction of complex **1** with NaO*t*Bu and $H_3B{\cdot}NMeH_2$ at 298 K. Bottom: *in situ* ^{1}H NMR spectrum (toluene-d_8, 400 MHz) at 207 K.

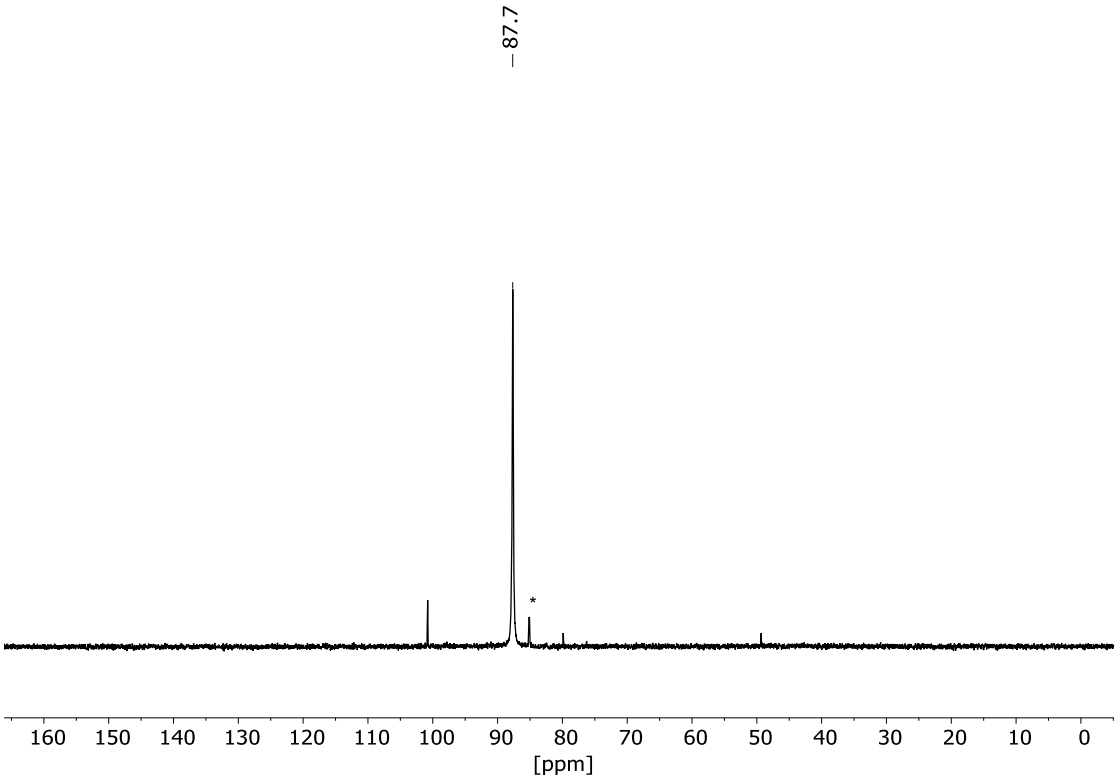

Figure S 10. *In situ* $^{31}P\{^{1}H\}$ NMR spectrum (toluene-d_8, 122 MHz, 298 K) of the reaction of complex **1** with NaO*t*Bu and $H_3B{\cdot}NMeH_2$. * complex **1**.

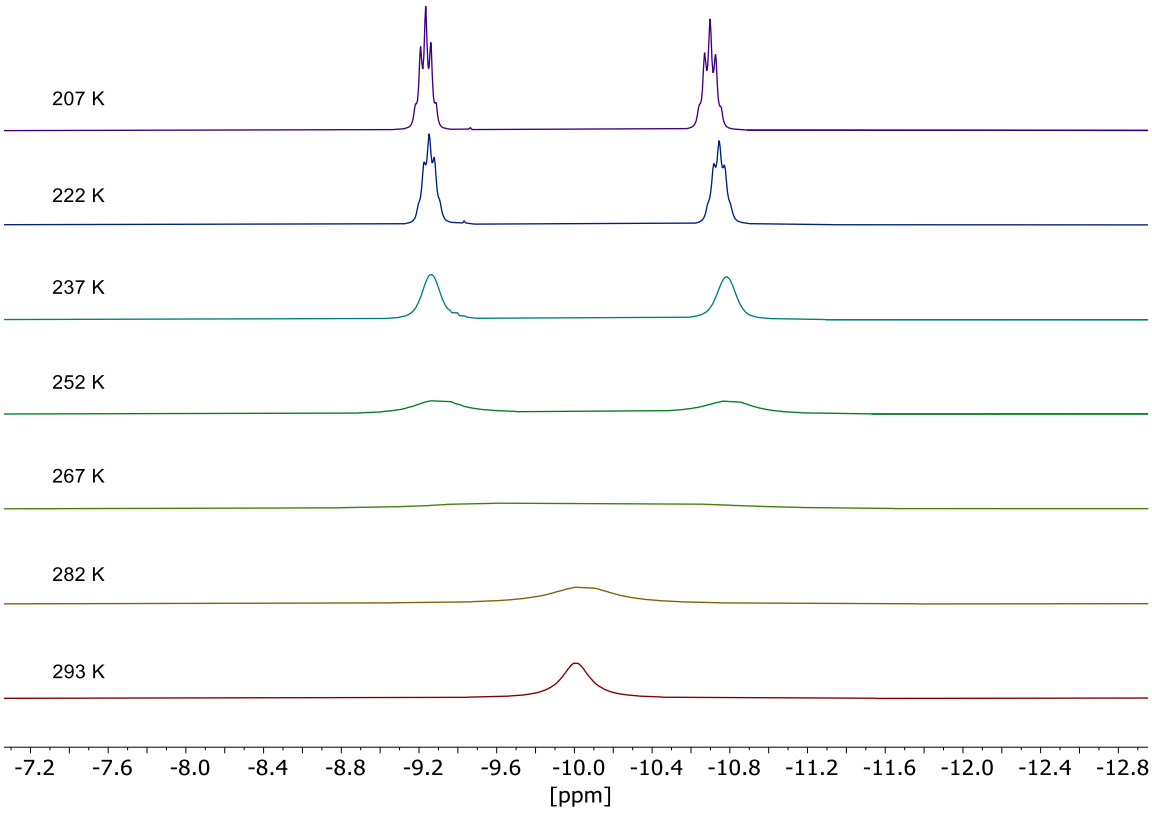

Figure S 11. Variable temperature ^{1}H NMR experiment (toluene-d_8, 400 MHz) of complex **4**.

Calculation of an estimated energy barrier for dynamic hydride exchange. For this estimation, the following empirical equation was used. It should be noted that the determination of the coalescence point is only a rough approximation which should be sufficient for a qualitative estimation of the calculated energies of the transition state (TS3).

$$\Delta G^{\#} = RT_C \left[22.96 + ln\left(\frac{T_C}{\delta\nu}\right)\right] \qquad \left|\frac{J}{mol}\right|$$

Equation S 1.

On the basis of the above shown variable temperature ^{1}H NMR experiment (Figure S 11) we estimated the coalescence temperature T_C = 267 K and the frequency as $\delta\nu_{203K}$ = 556 Hz.[7]

$$\Delta G^{\#} = (8.314\,J\,K^{-1}\ mol^{-1})(267\,K)\left[22.96 + ln\left(\frac{267\,K}{556\,s^{-1}}\right)\right] = 49339\,J\,mol^{-1} = 49.3\,kJ\,mol^{-1}$$

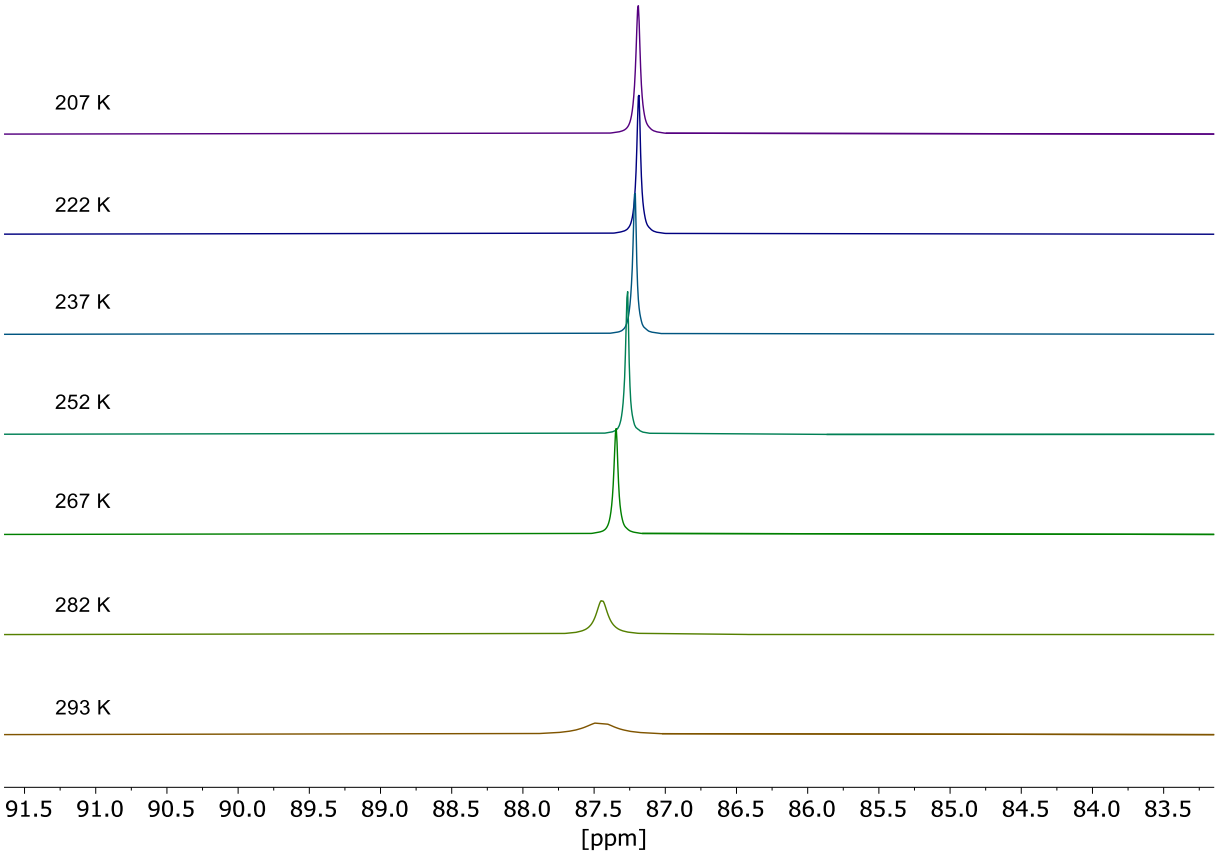

Figure S 12. Variable temperature ^{31}P{^{1}H} NMR experiment (toluene-d_8, 162 MHz) of complex **4**.

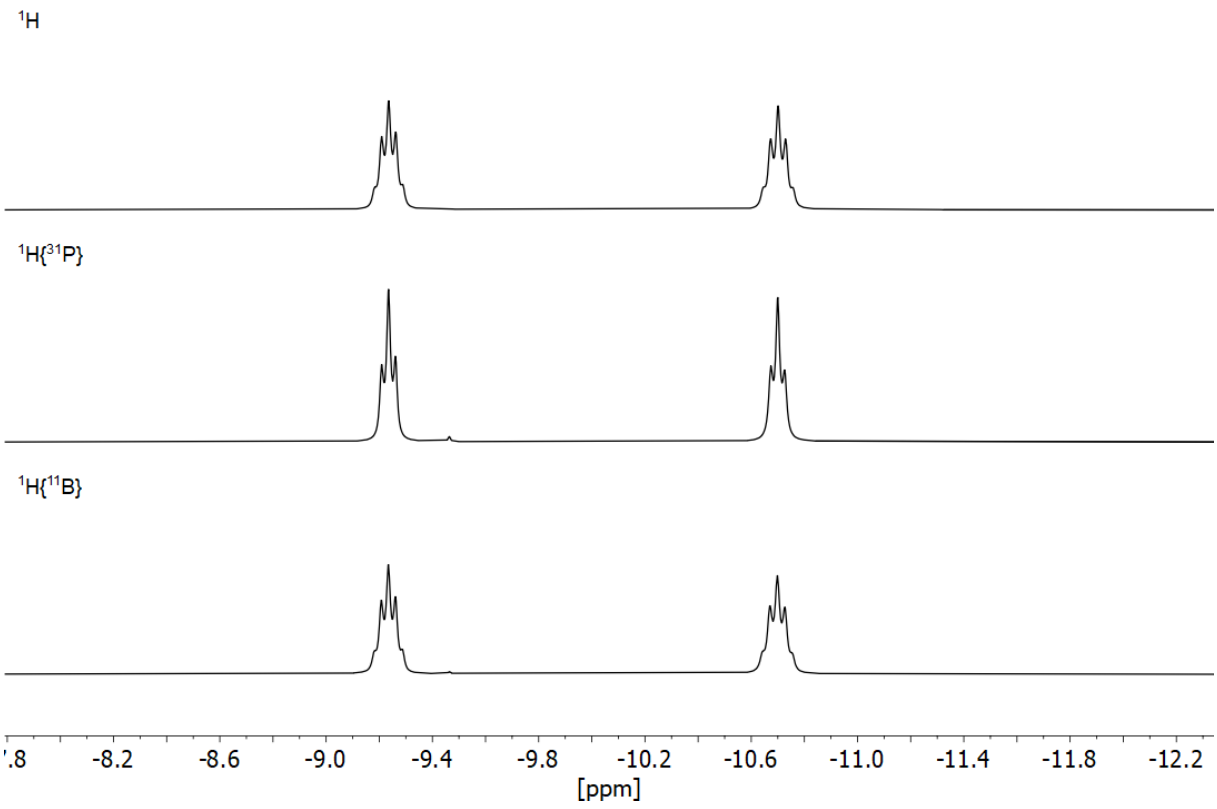

Figure S 13. ^{1}H, ^{1}H{^{31}P} and ^{1}H{^{11}B} NMR spectra (toluene-d_8, 207 K, 400 MHz) of complex **4**.

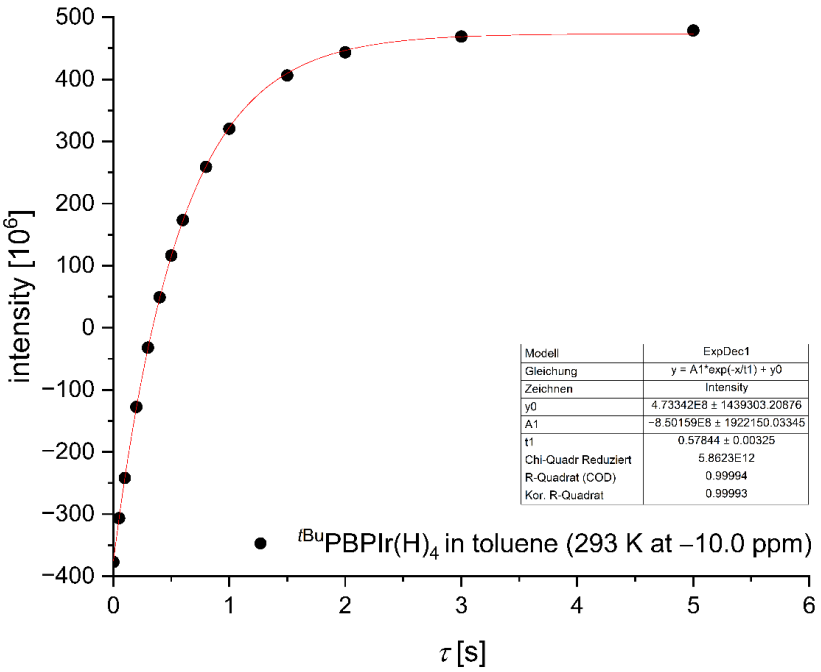

Figure S 14. Estimation of the longitudinal relaxation time T_1 for the hydride ligand (−10.0 ppm) by the inversion recovery sequence of **4** in toluene-d_8 at 293 K.

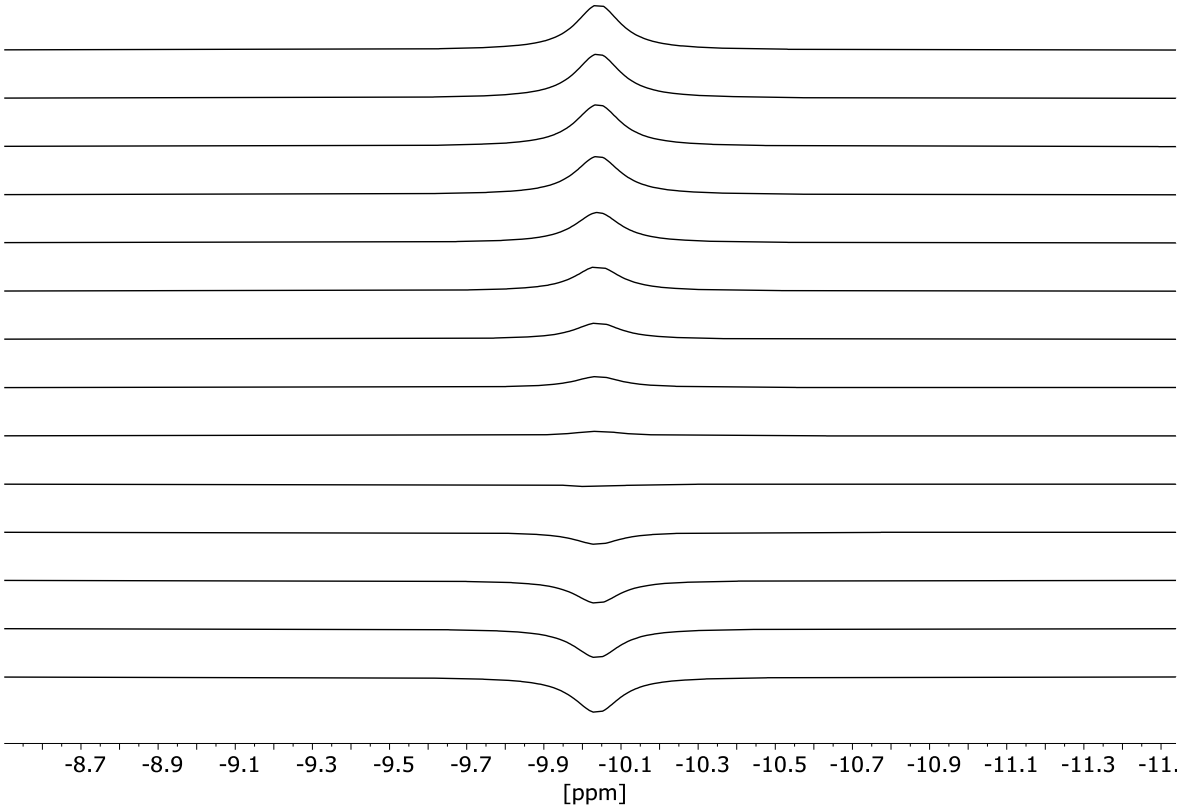

Figure S 15. $^{1}H\{^{31}P\}$ inversion recovery experiment of hydride signal (−10.0 ppm) in toluene-d_8 at 293 K of **4**.

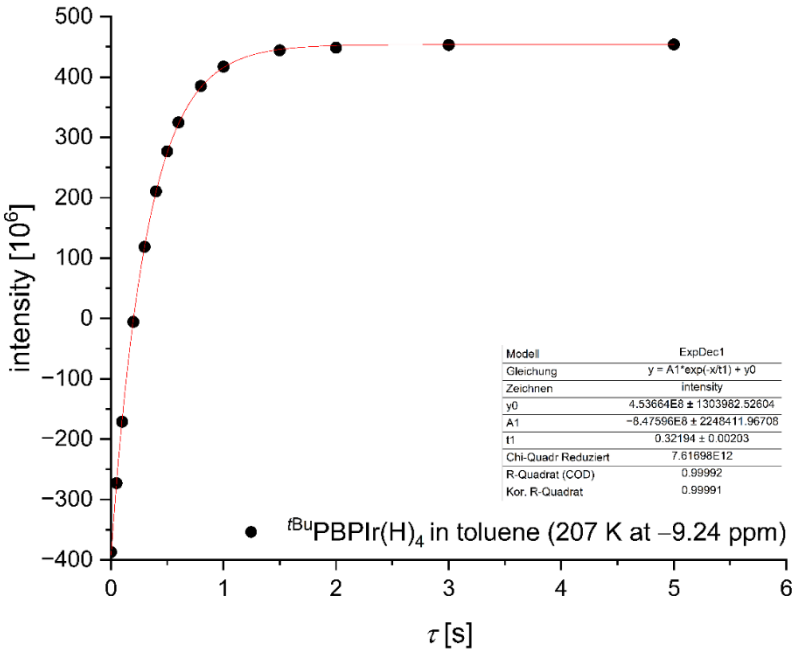

Figure S 16. Estimation of the longitudinal relaxation time T_1 for the hydride ligand (−9.24 ppm) by the inversion recovery sequence of **4** in toluene-d_8 at 207 K.

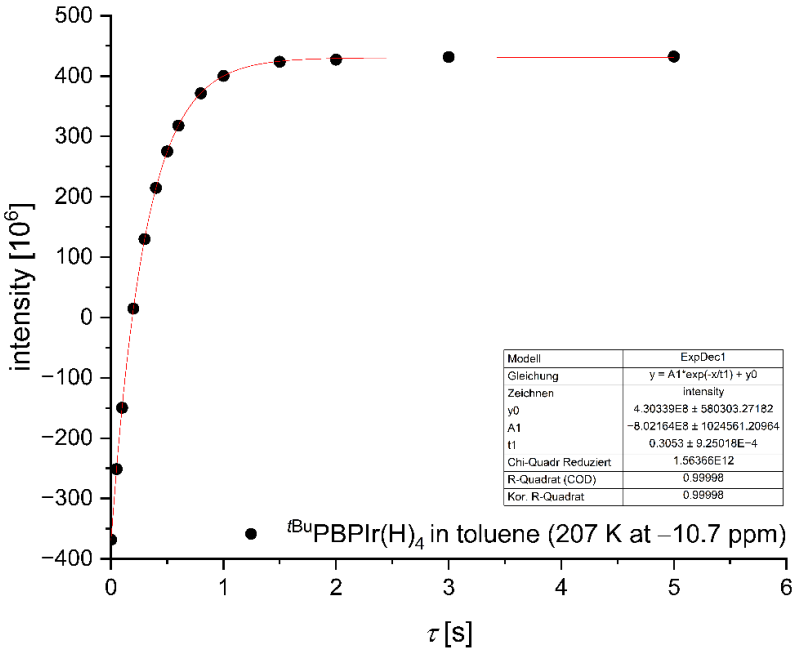

Figure S 17. Estimation of the longitudinal relaxation time T_1 for the hydride ligand (−10.7 ppm) by the inversion recovery sequence of **4** in toluene-d_8 at 293 K.

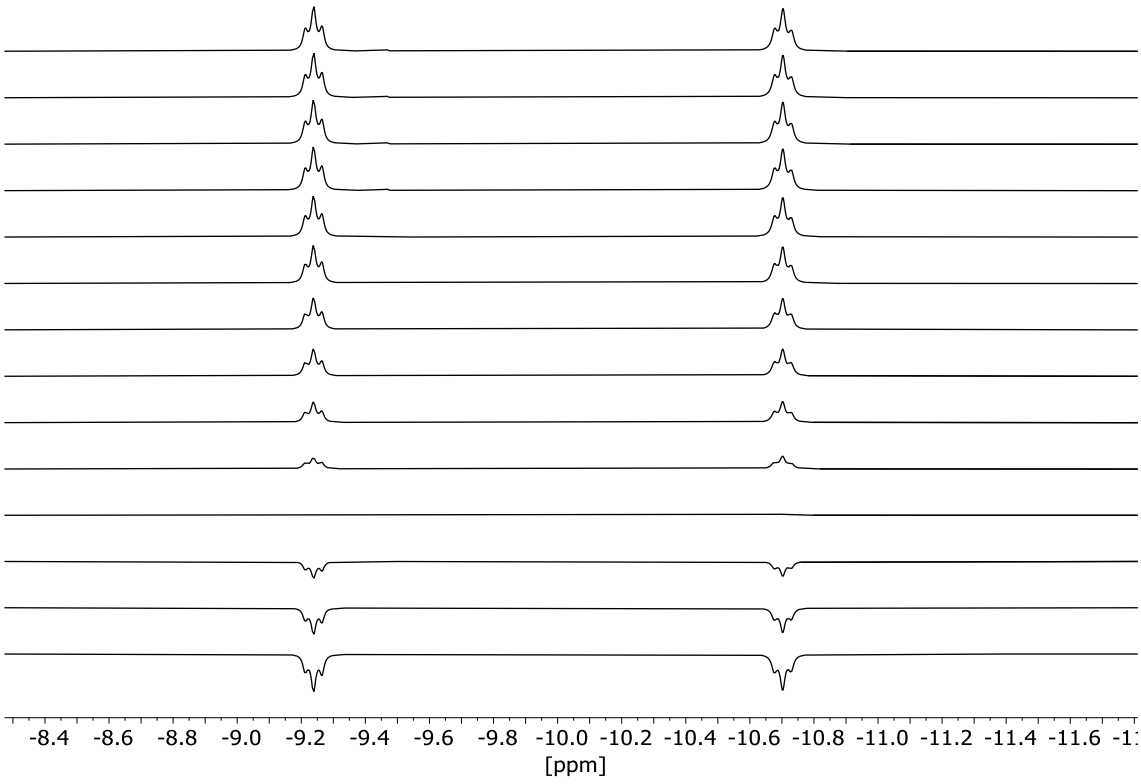

Figure S 18. $^1H\{^{31}P\}$ inversion recovery experiment of hydride signals (−9.24 and −10.7 ppm) in toluene-d_8 at 207 K of **4**.

3.4 Deuteration experiments – Reaction of complex 1 with $D_3B{\cdot}NMeH_2$ and NaO*t*Bu

Precatalyst **1** (35.0 mg, 45.3 µmol), $D_3B{\cdot}NMeH_2$ (2.17 mg, 45.3 µmol) and NaO*t*Bu (4.57 mg, 47.6 µmol) were dissolved in toluene-d_8 (0.7 mL) in a Young-NMR-tube. The colour of the reaction mixture turns from yellow to dark brown after a few minutes. ^{1}H NMR monitoring of the progress of the reaction shows a broad singlet at −10.0 ppm.

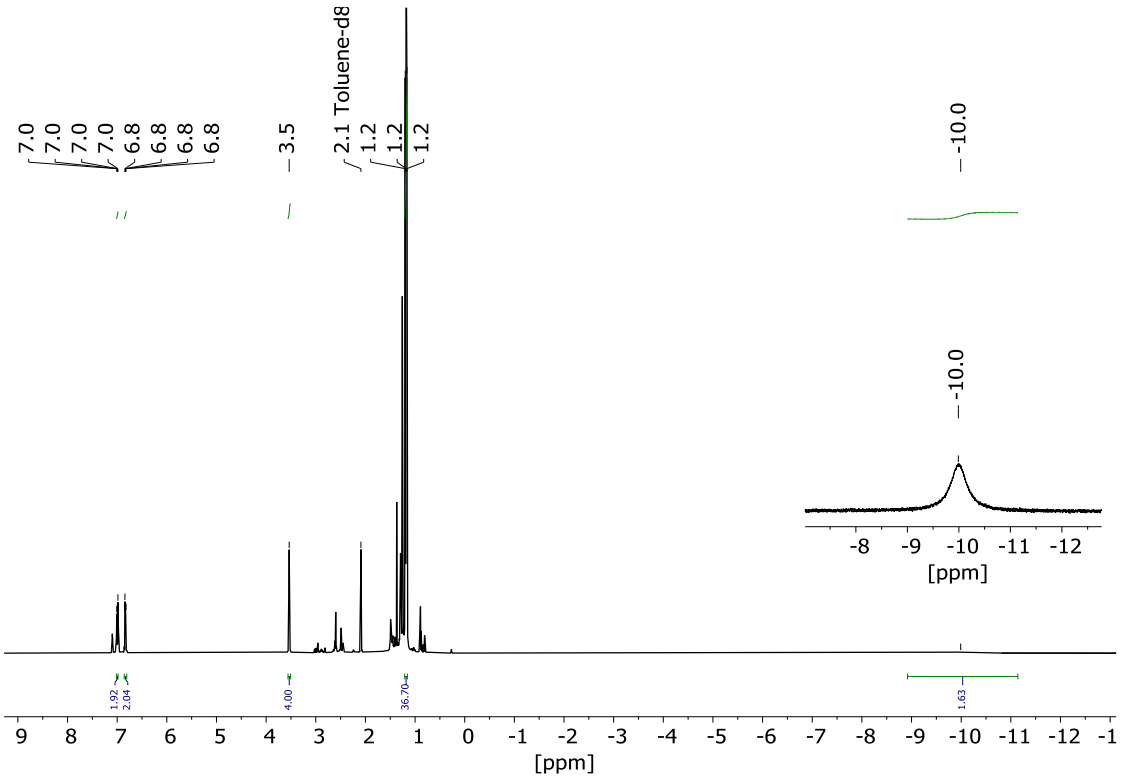

Figure S 19. ^{1}H NMR spectrum (toluene-d_8, 400 MHz, 298 K) of the reaction of complex **1** with NaO*t*Bu and $D_3B{\cdot}NMeH_2$.

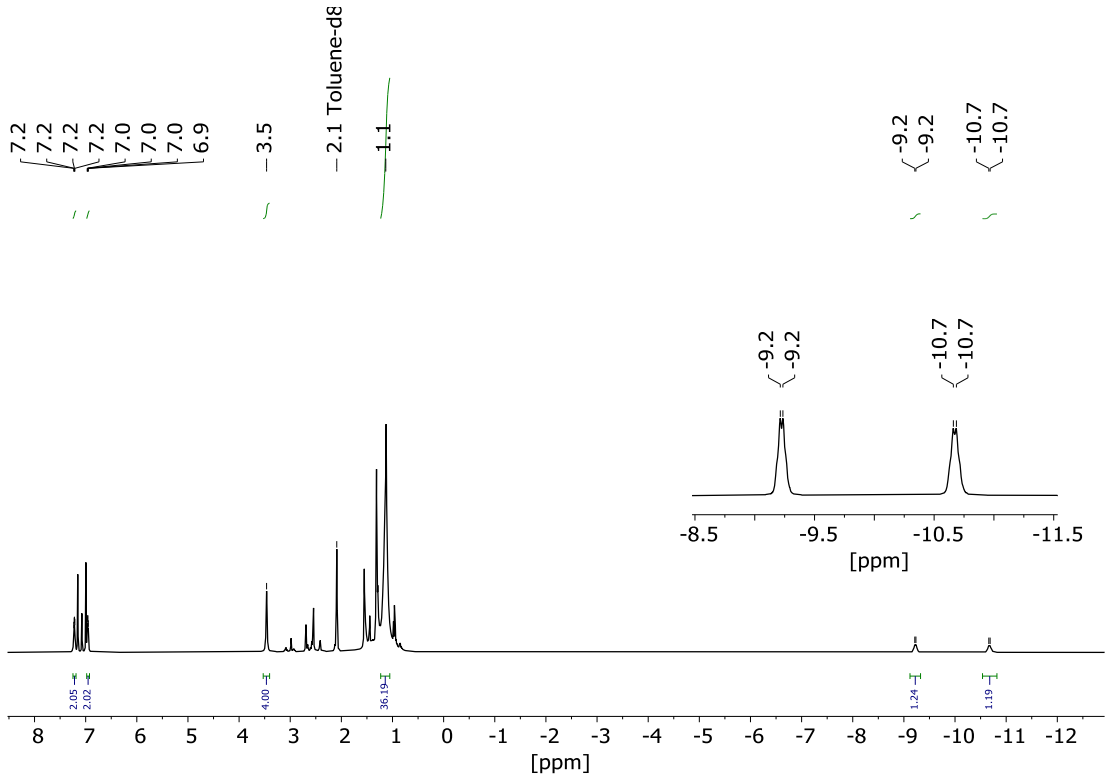

Figure S 20. ^{1}H NMR spectrum (toluene-d_8, 400 MHz, 203 K) of the reaction of complex **1** with NaO*t*Bu and $D_3B{\cdot}NMeH_2$. Hydride signals at δ -9.2 ppm, -10.7 ppm.

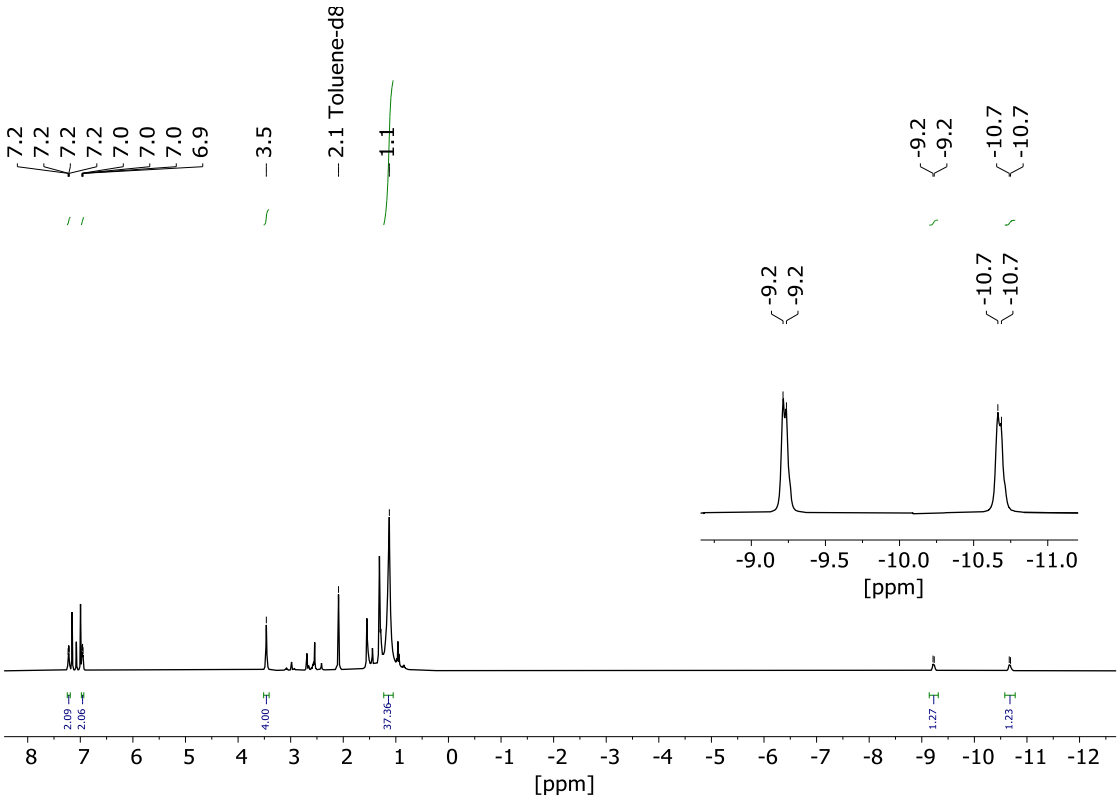

Figure S 21. ^{1}H{^{31}P} NMR spectrum (toluene-d_8, 400 MHz, 203 K) of the reaction of complex **1** with NaO*t*Bu and $D_3B{\cdot}NMeH_2$. Hydride signals at δ -9.2 ppm, -10.7 ppm.

3.5 Deuteration experiments – Reaction of 4 with D_2

Precatalyst **1** (35.0 mg, 45.3 µmol), $H_3B{\cdot}NMeH_2$ (2.03 mg, 45.3 µmol) and NaO*t*Bu (4.57 mg, 47.6 µmol) were dissolved in toluene-d_8 (0.7 mL) in a Young-NMR-tube. The colour of the reaction mixture turns from yellow to dark brown after a few minutes. The reaction mixture was frozen, degassed (3x) and the H_2 atmosphere was exchanged with D_2 gas. The reaction mixture was then analysed by NMR experiments at 203 K and room temperature.

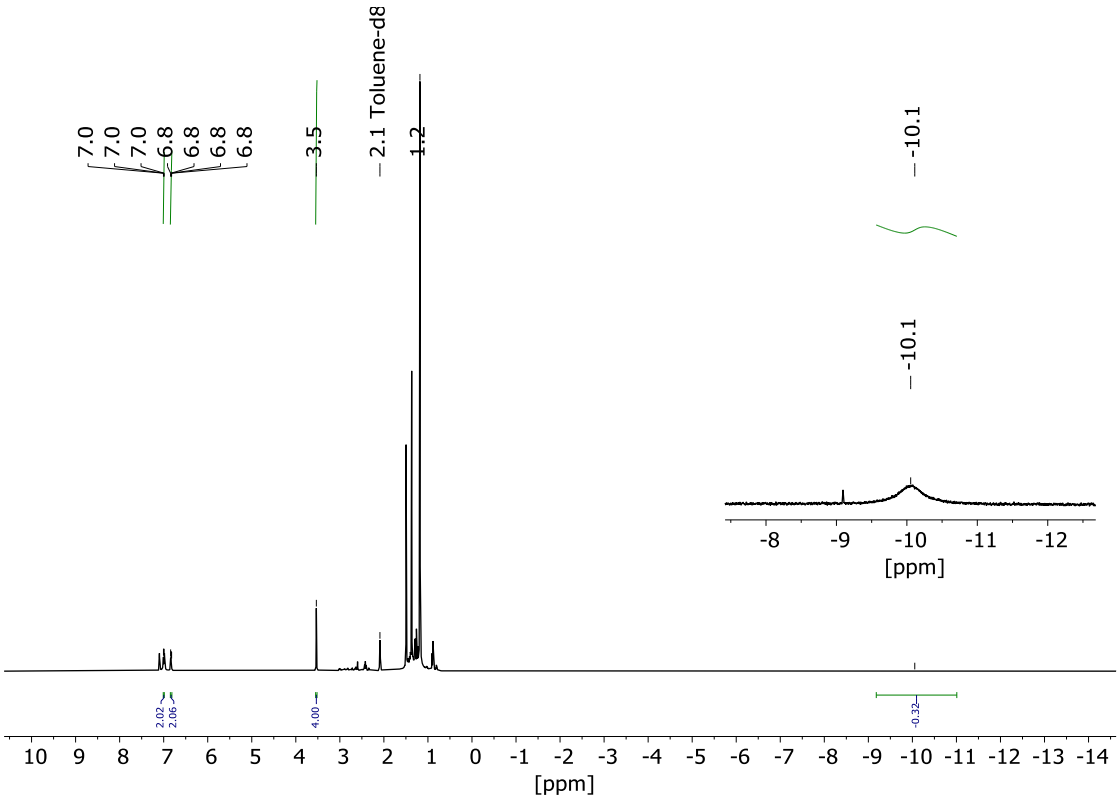

Figure S 22. ^{1}H NMR spectrum (toluene-d_8, 400 MHz, 298 K) of complex **4** after gas exchange with D_2 at room temperature.

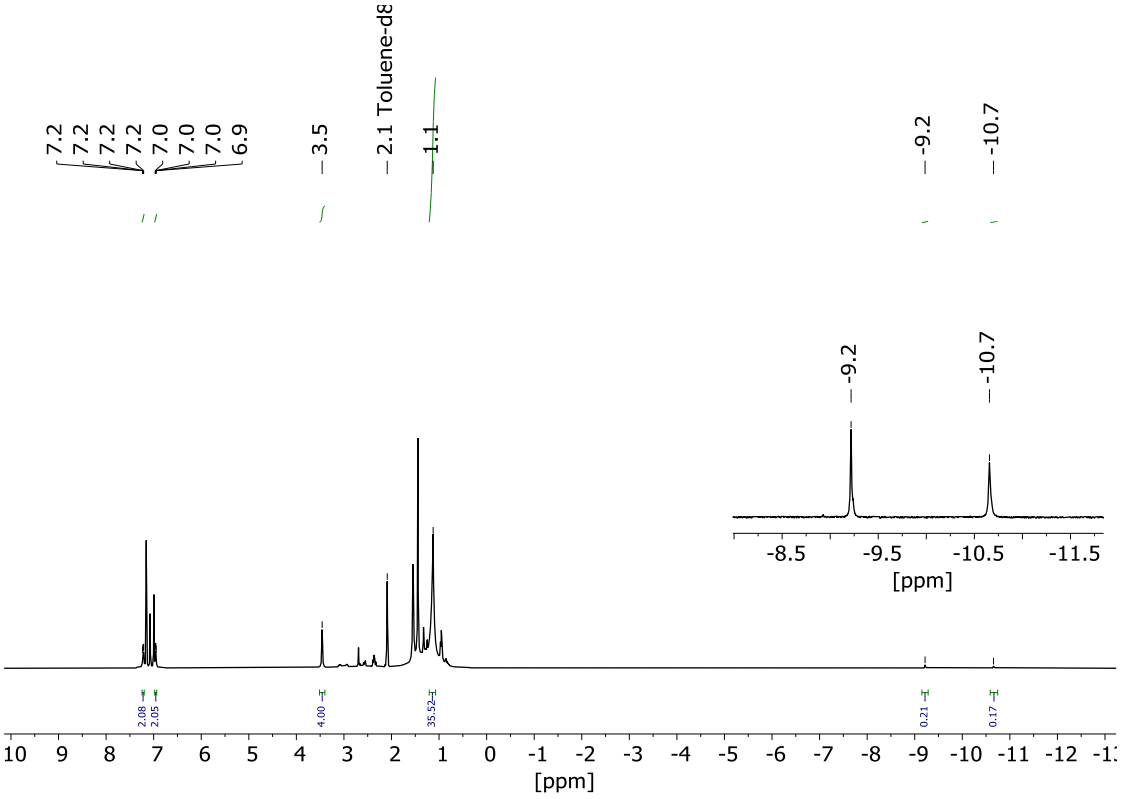

Figure S 23. $^{1}H\{^{31}P\}$ NMR spectrum (toluene-d_8, 400 MHz, 203 K) of complex **4** after gas exchange with D_2 at room temperature.

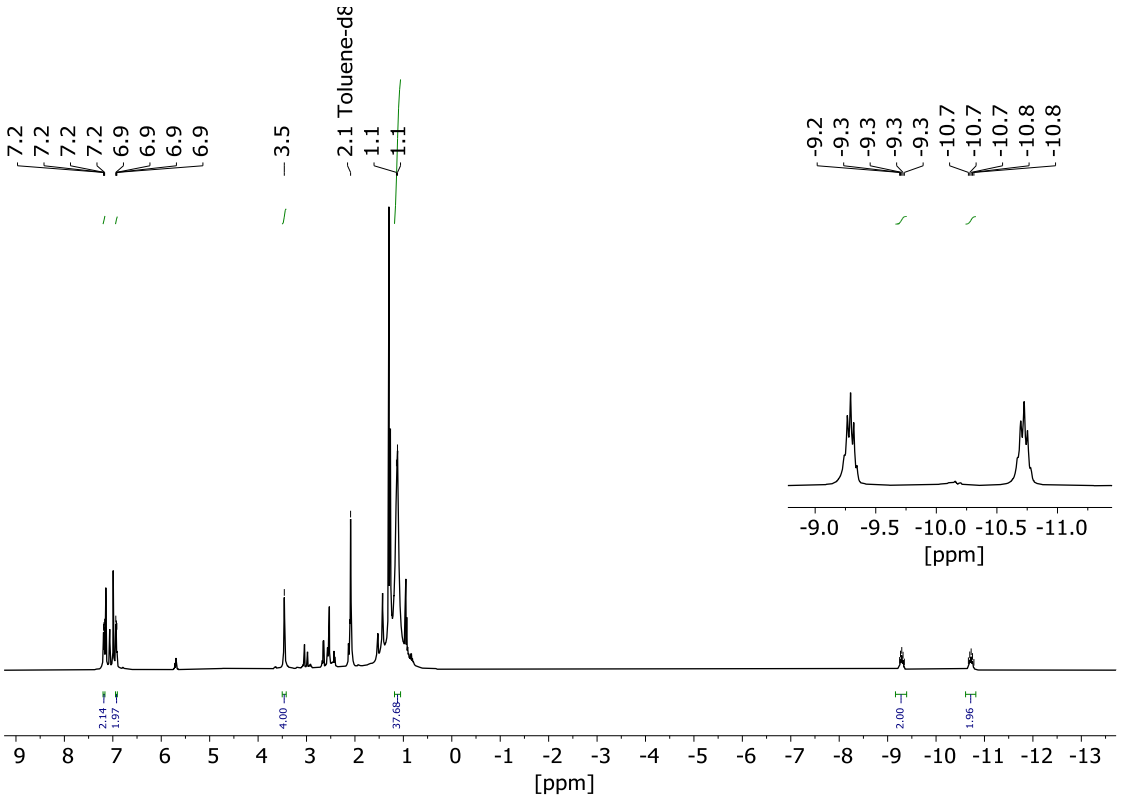

Figure S 24. ^{1}H NMR spectrum (toluene-d_8, 400 MHz, 203 K) of complex **4** after gas exchange with D_2 at -78 °C.

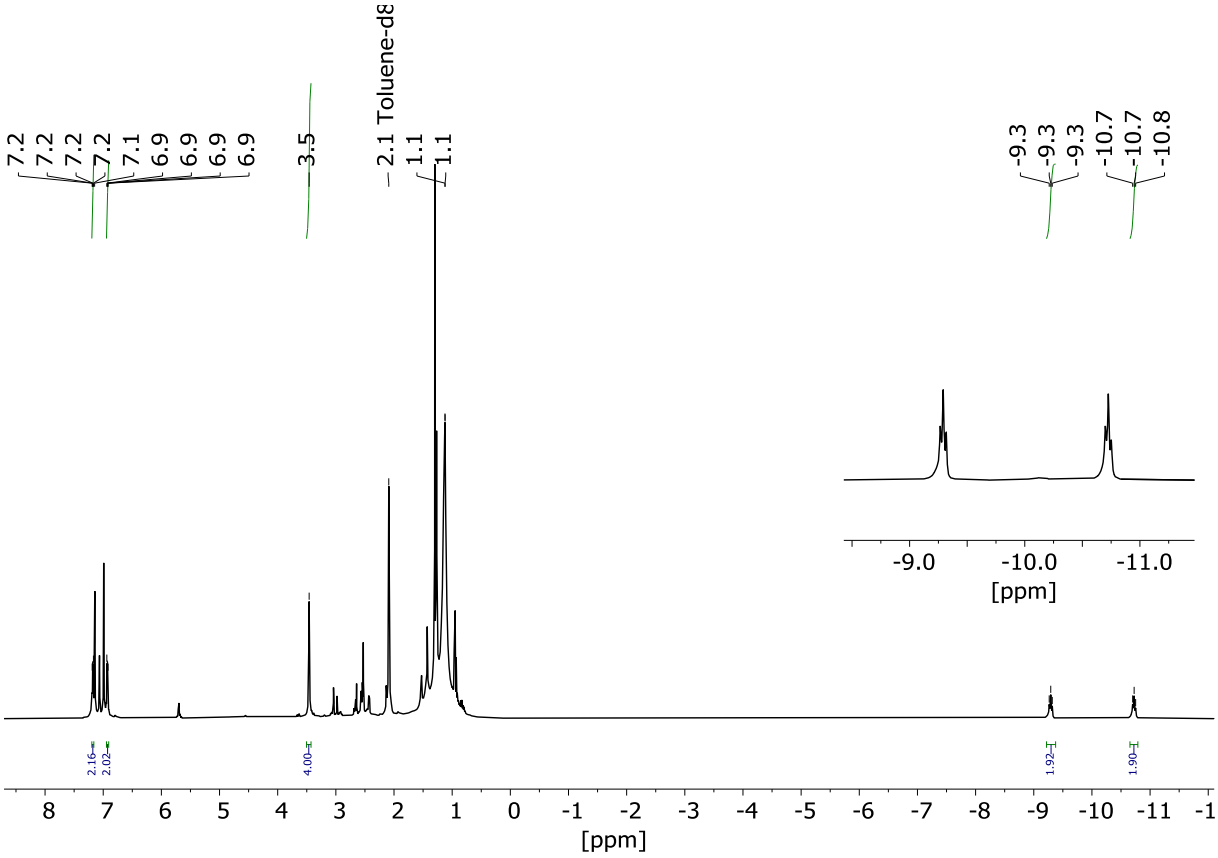

Figure S 25. $^{1}H\{^{31}P\}$ NMR spectrum (toluene-d_8, 400 MHz, 203 K) of complex **4** after gas exchange with D_2 at -78 °C.

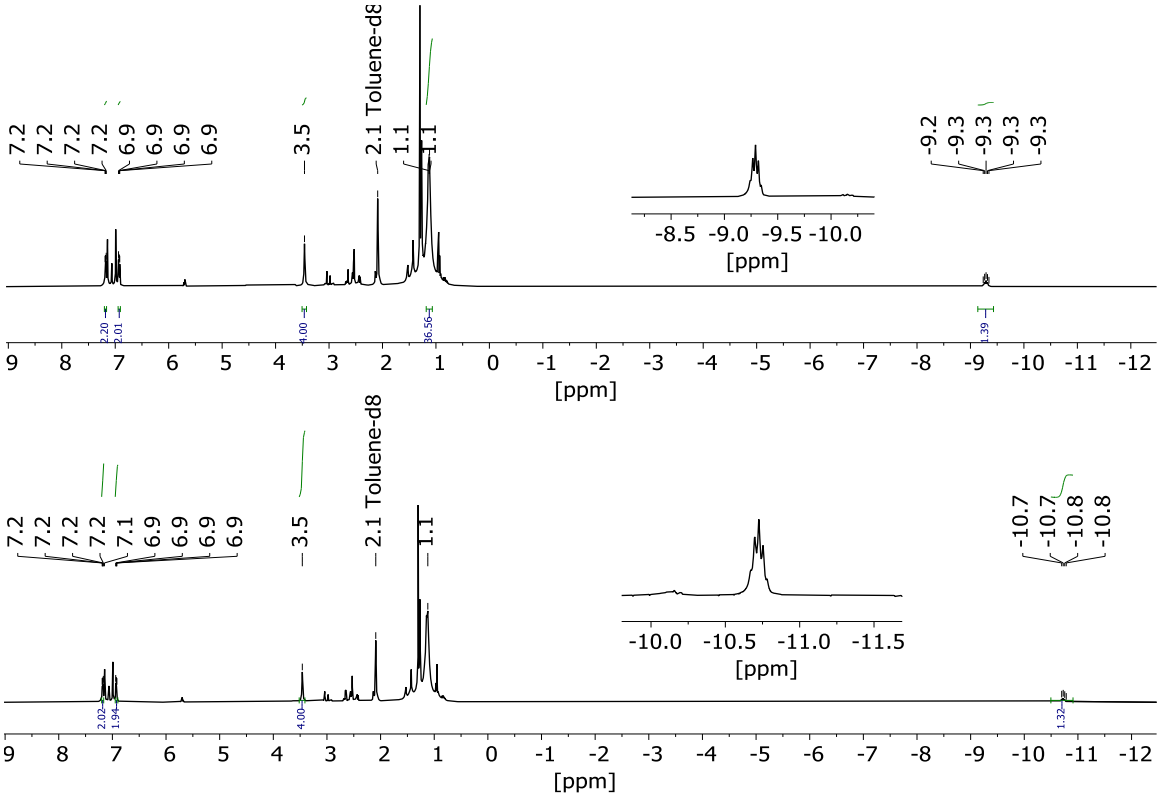

Figure S 26. ^{1}H saturation transfer experiment (toluene-d_8, 400 MHz, 203 K) of the gas exchange reaction with D_2 at −78°C with complex **4**, performed at the hydride signals. Top: Presaturation at −10.74 ppm. Bottom: Presaturation at −9.30 ppm. In both cases, the intensity of the other hydride signal is clearly reduced. Selectivity of the saturation was proven by irradiation at –7.68 ppm which has no effect.

3.6 Reaction of complex 1 with LiTMP and H_2

Complex **1** (24.8 mg, 34.5 µmol) and LiTMP (1.05 eq.,1.61 mg, 39.3 µmol) were dissolved in toluene-d_8 (0.7 mL) in a Young-NMR-tube. The reaction mixture was degassed (three freeze-pump-thaw-cycles). Then the reaction mixture was frozen at −196°C, evacuated, followed by purging with H_2 gas. The mixture was then allowed to slowly warm to room temperature under vigorous stirring. This H_2 purging cycle was repeated at least three times. Afterwards the reaction mixture was stirred at 90°C overnight. The colour of the reaction mixture turns from yellow to dark brown. ^{1}H NMR monitoring of the reaction solution shows a broad singlet at −10.1 ppm.

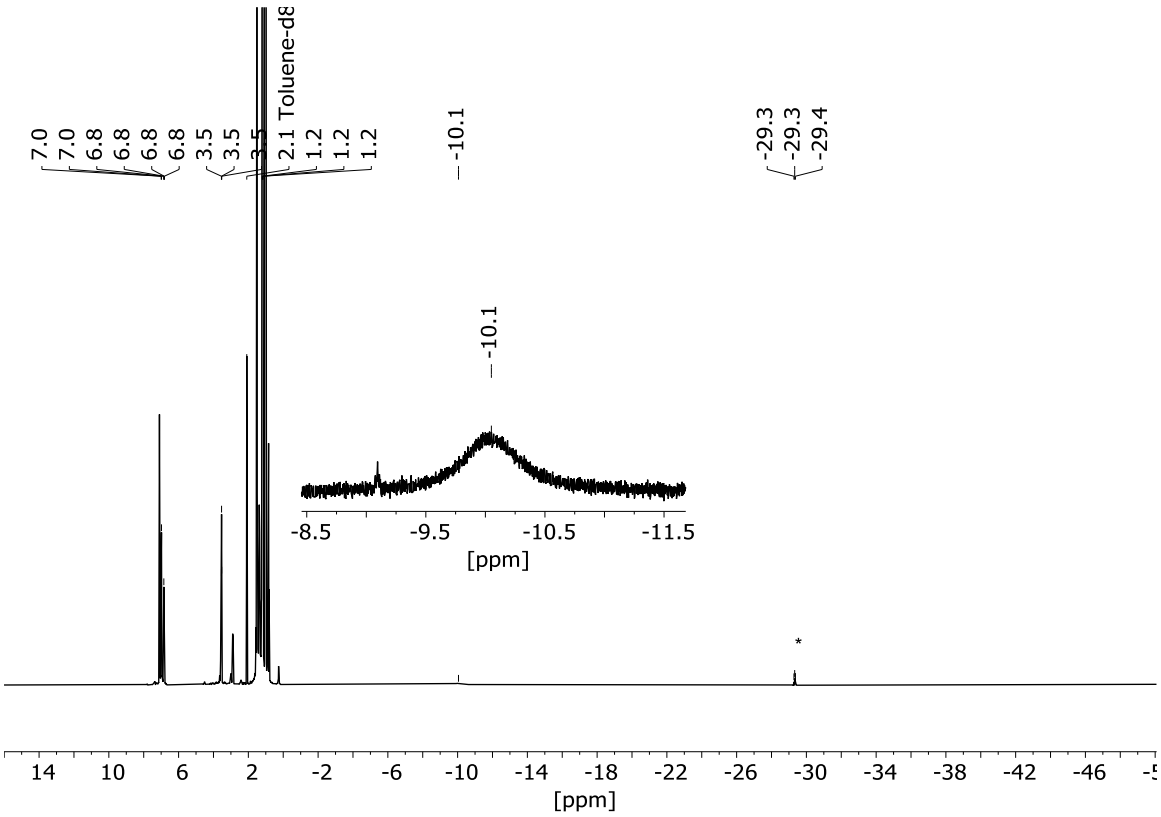

Figure S 27. ^{1}H NMR spectrum (toluene-d_8, 300 MHz, 298 K) of the reaction of complex **1** with LiTMP and H_2. * complex **1**.

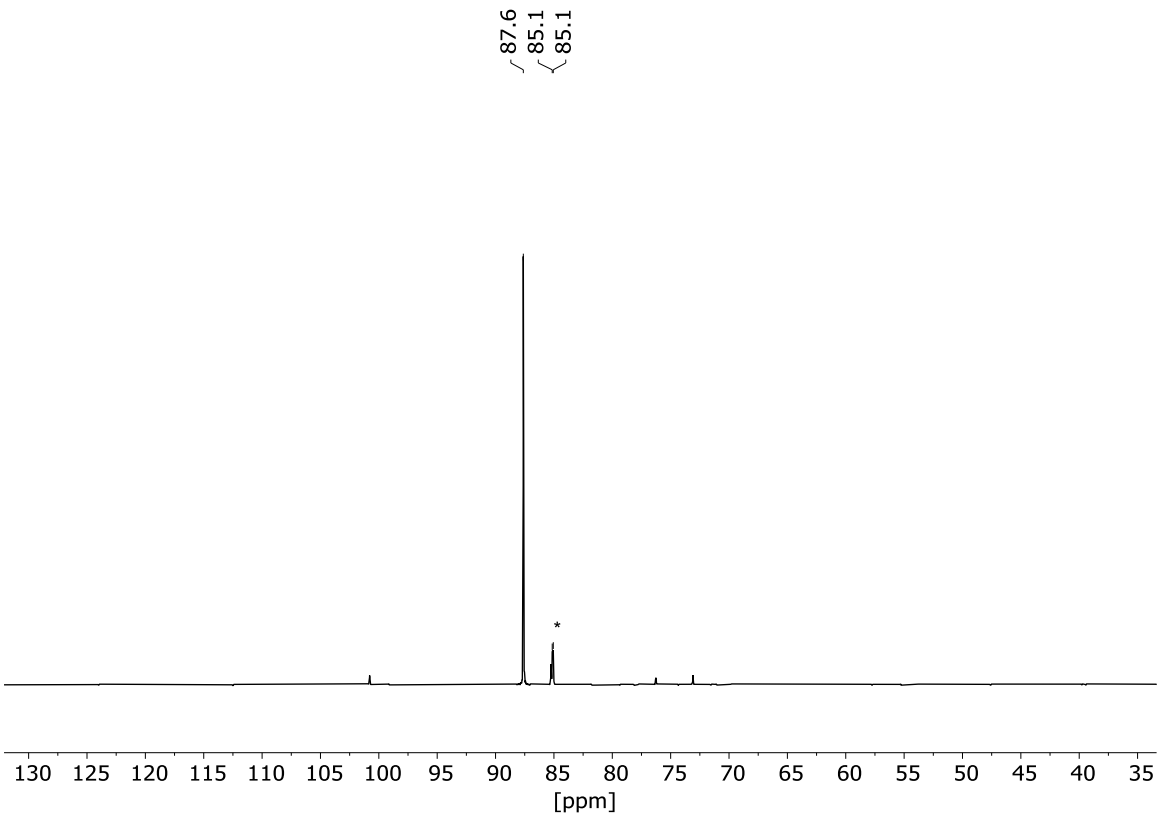

Figure S 28. ^{31}P{^{1}H} NMR spectrum (toluene-d_8, 122 MHz, 298 K) of the reaction of complex **1** with LiTMP and H_2. * complex **1**.

3.7 Reaction of 1 (5 mol%) with $H_3B{\cdot}NMeH_2$

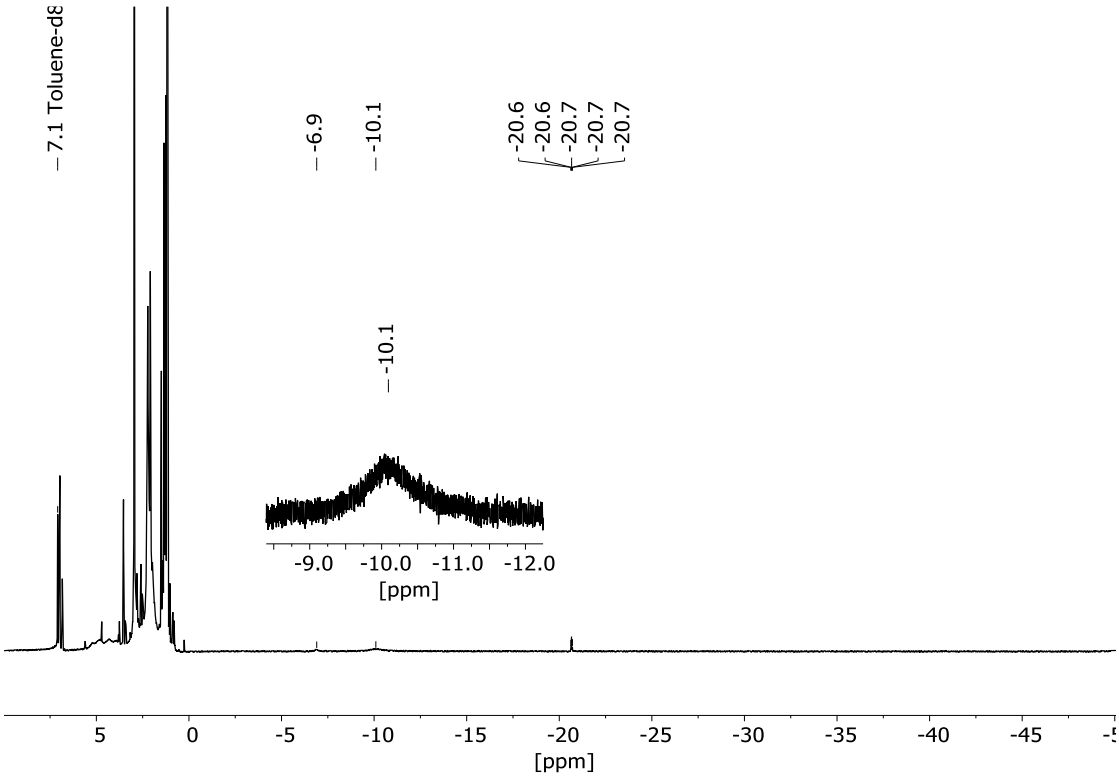

Figure S 29. ^{1}H NMR spectrum (toluene-d_8, 300 MHz, 298 K) of the reaction of **1** (5 mol%) with $H_3B{\cdot}NMeH_2$.

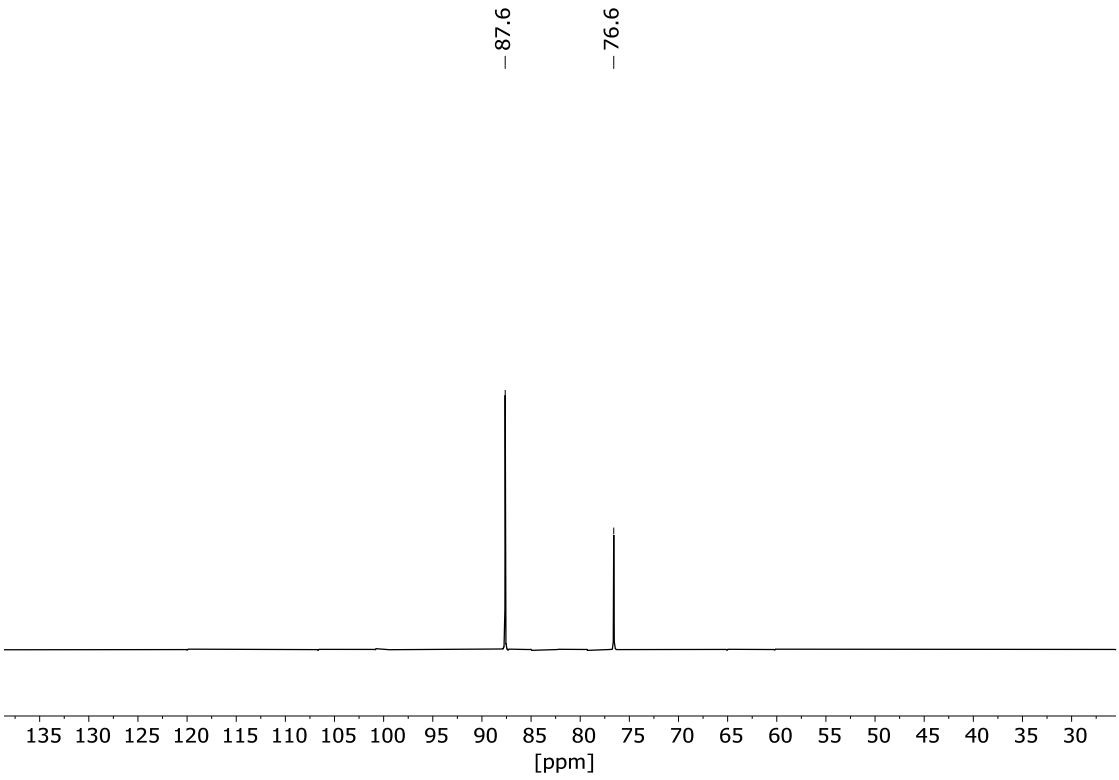

Figure S 30. $^{31}P\{^{1}H\}$ NMR spectrum (toluene-d_8, 122 MHz, 298 K) of the reaction of **1** (5 mol%) with $H_3B{\cdot}NMeH_2$.

4 Dehydrocoupling of amine boranes

4.1 General procedure

$H_3B{\cdot}NH_3$ or $H_3B{\cdot}NMeH_2$ (1.33 mmol), NaO*t*Bu (1 mol%) and the corresponding precatalyst (1 mol%) were weighed into a three-necked reaction vessel. The reaction vessel was connected to an automatically operating gas buret[8] under Ar atmosphere. The gas buret was initialised, the solvent (THF or toluene, 10 mL) was added, and the data acquisition was started immediately. After the reaction, a gas sample was taken and analysed by TCD-GC to confirm the presence of H_2. An aliquot was taken from the reaction mixture and analysed by NMR spectroscopy (^1H, $^{31}P\{^1H\}$, ^{11}B, $^{11}B\{^1H\}$).

4.2 Overview of the catalytic conditions

Table S 3. Overview of the catalytic conditions for the dehydrocoupling of amine boranes.

entry	catalyst	*c* / mol%	substrate	solvent	reaction time / h	equivalent H_2
1	**1**	1.0	$H_3B{\cdot}NMeH_2$	toluene	1.25	0.85
2	**1**	2.0	$H_3B{\cdot}NMeH_2$	toluene	0.20	0.92
3	**1**	1.0	$H_3B{\cdot}NMeH_2$	THF	44.4	0.88
4	**1**	2.0	$H_3B{\cdot}NMeH_2$	THF	88.5	0.94
5[a]	**2**	1.0	$H_3B{\cdot}NMeH_2$	toluene	25.0	0.78
6[a]	**3**	1.0	$H_3B{\cdot}NMeH_2$	toluene	12.5	0.90
7[a]	**3**	0.1	$H_3B{\cdot}NMeH_2$	toluene	50.0	0.89
8	**1**	1.0	$H_3B{\cdot}NH_3$	THF	60.0	1.03
9	**1**	1.0	$H_3B{\cdot}NH_3$	toluene	93.0	0.85
10[a]	**2**	1.0	$H_3B{\cdot}NH_3$	THF	45.0	0.53

Reaction conditions: *c*(substrate) = 1.33 M, *V*(Solvent) = 10 mL, 1 eq. NaO*t*Bu. [a] Without the use of NaO*t*Bu.

4.3 Dehydrocoupling of $H_3B{\cdot}NMeH_2$

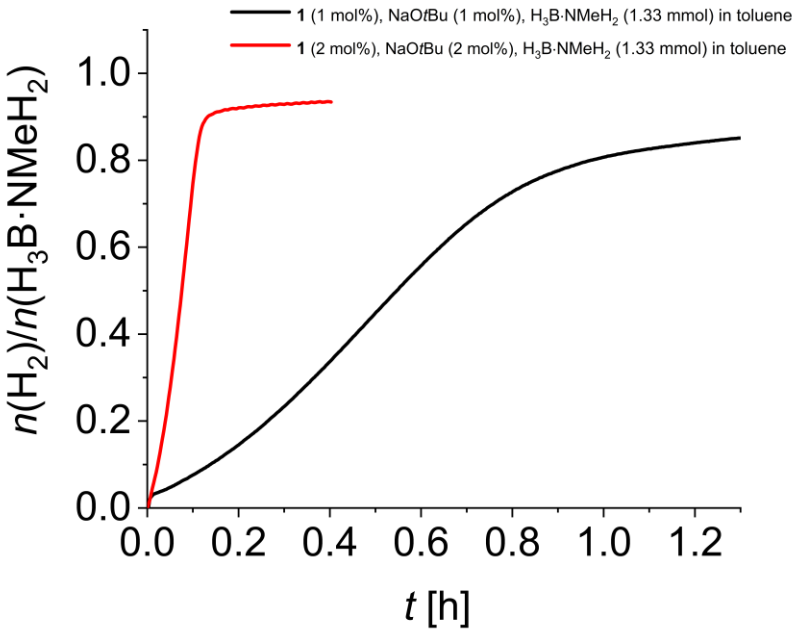

Figure S 31. Volumetric curves of the dehydrocoupling of $H_3B{\cdot}NMeH_2$ with complex **1** and NaO*t*Bu.

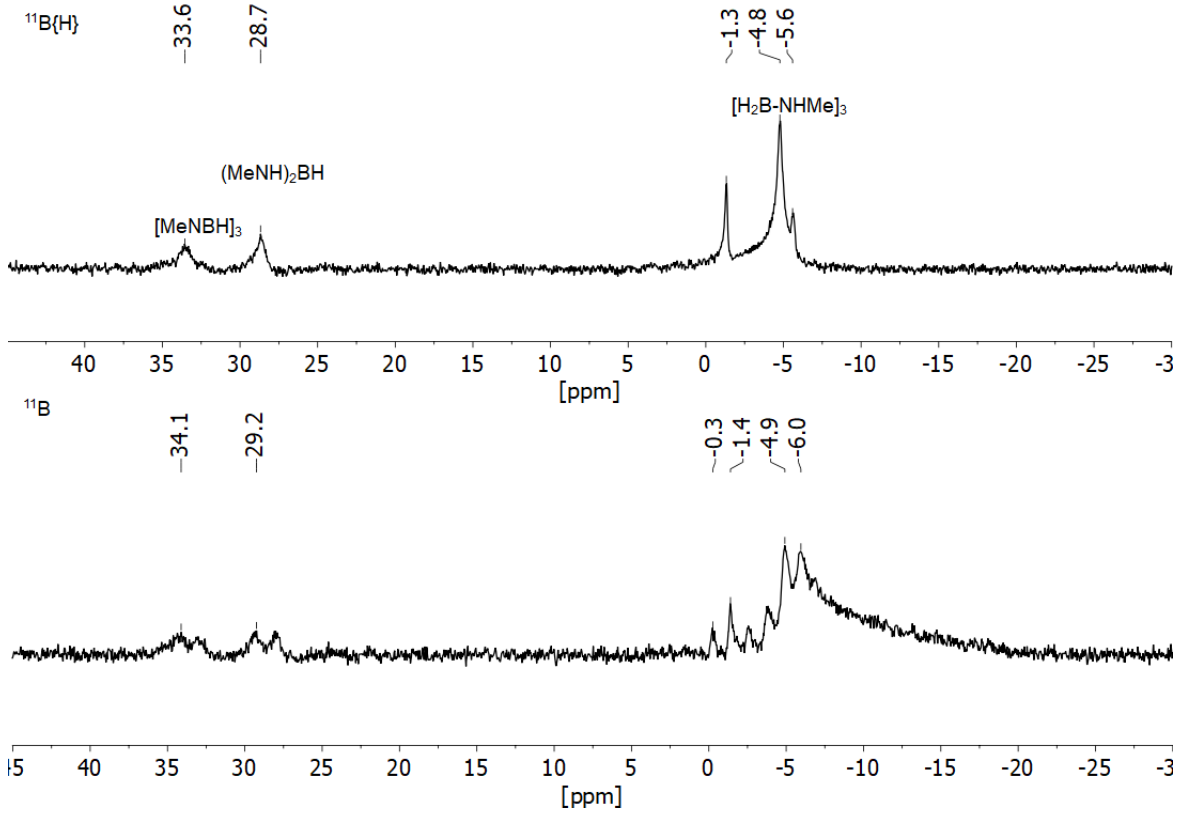

Figure S 32. $^{11}B\{^1H\}$ and ^{11}B NMR spectra (96 MHz, toluene-d_8) of dehydrocoupling of $H_3B{\cdot}NMeH_2$ with complex **1**. Conditions: T = 25°C, toluene, 1 mol% NaO*t*Bu, 1 mol% **1**.

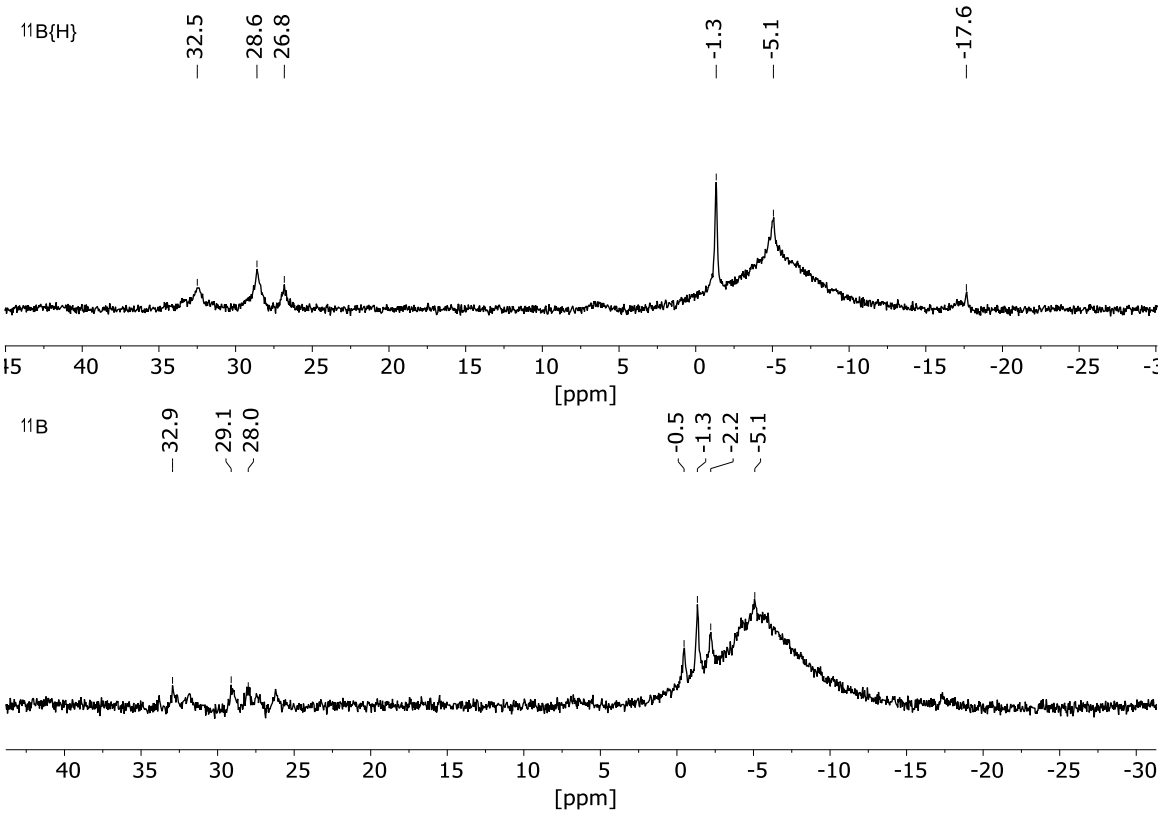

Figure S 33. $^{11}B\{^{1}H\}$ and ^{11}B NMR spectra (128 MHz, toluene-d_8) of dehydrocoupling of $H_3B{\cdot}NMeH_2$ with complex **1**. Conditions: *T* = 25°C, toluene, 2 mol% NaO*t*Bu, 2 mol% **1**.

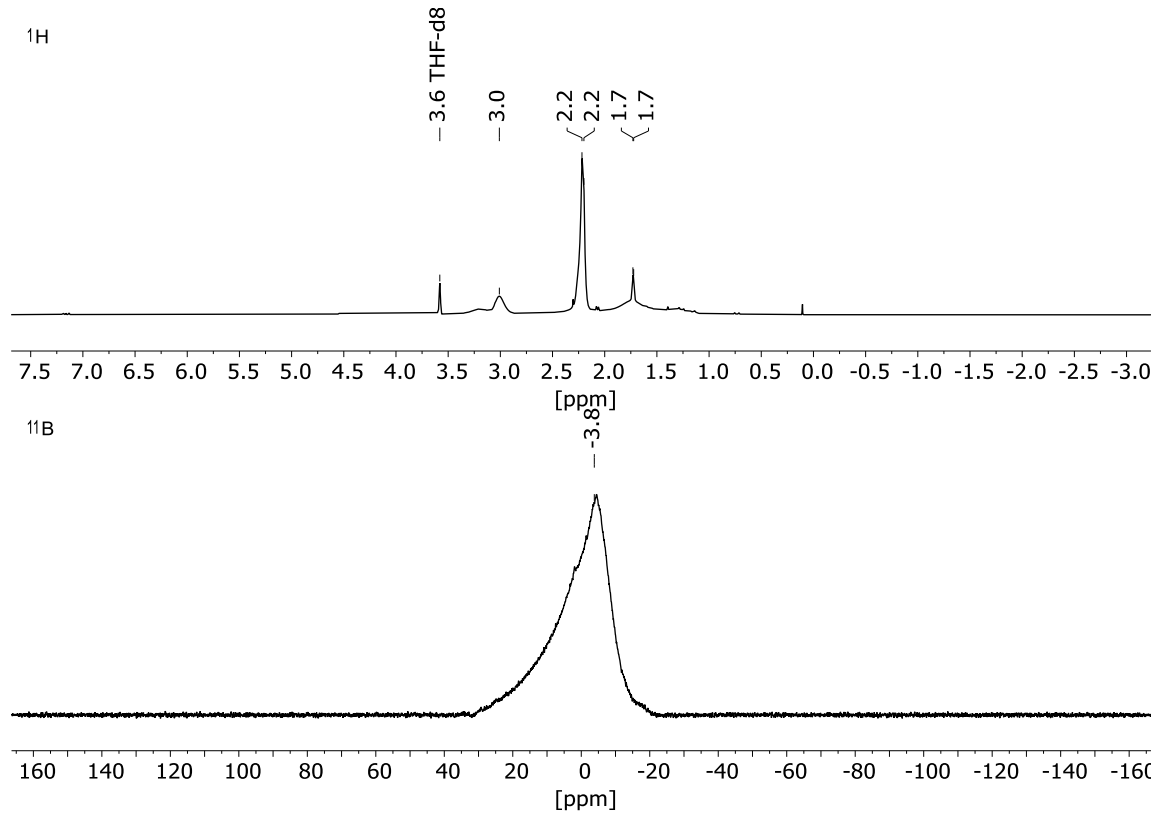

Figure S 34. ^{1}H (300 MHz) and ^{11}B NMR spectra (96 MHz) in THF-d_8 of isolated $(H_2B{\cdot}NMeH)_n$. Conditions: *T* = 25°C, toluene, 2 mol% NaO*t*Bu, 2 mol% **1**.

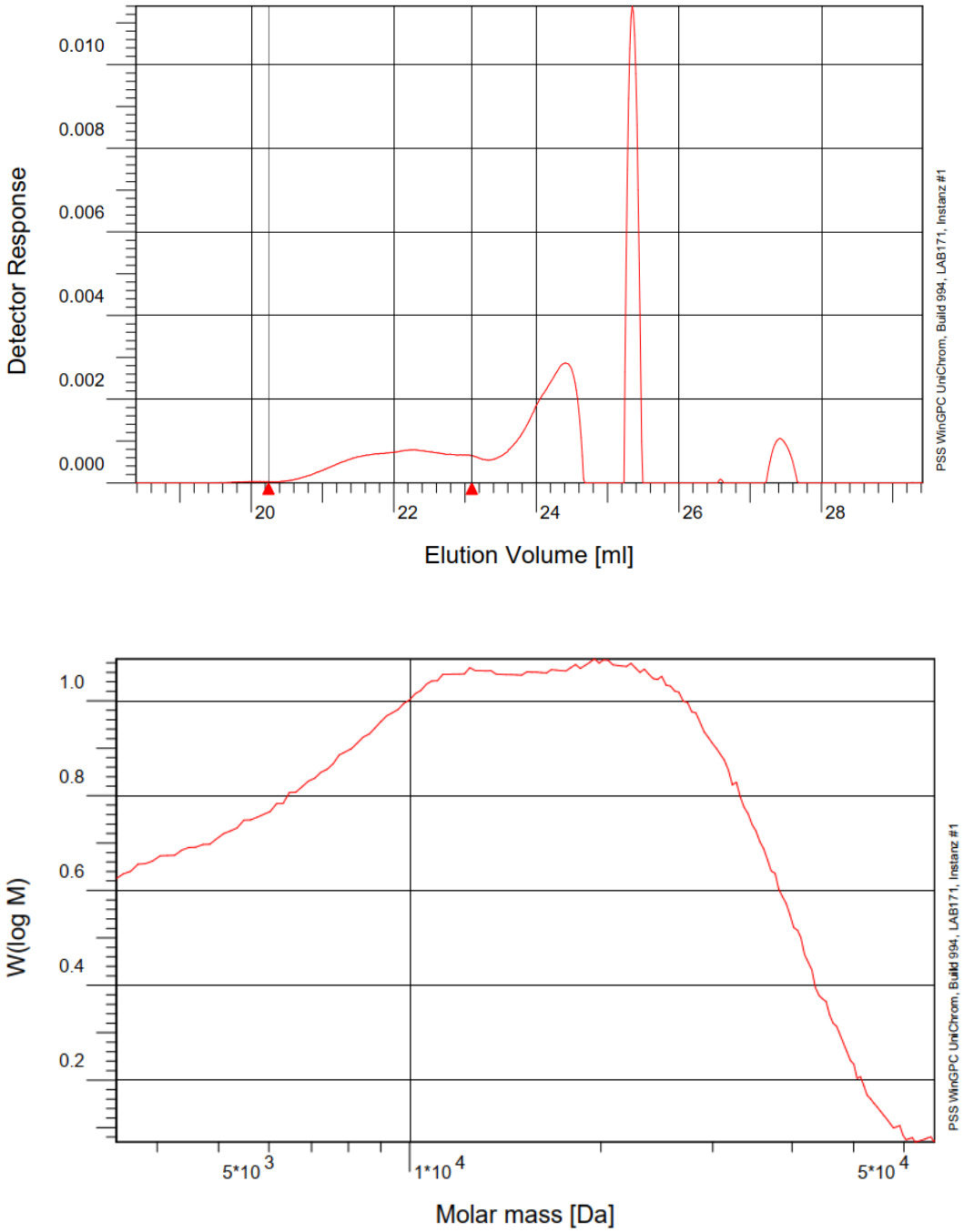

Figure S 35. SEC data of isolated polymer from the dehydropolymerisation of $H_3B{\cdot}NMeH_2$ with 2 mol% **1**.

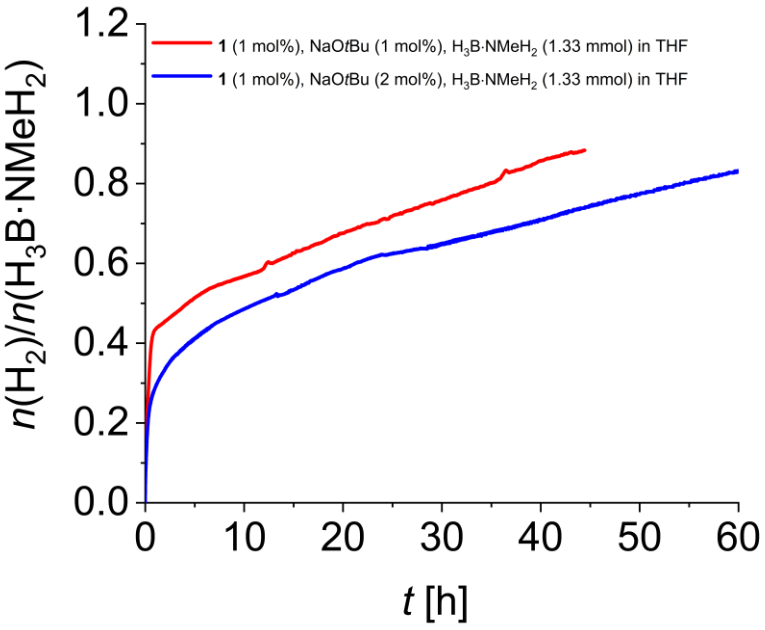

Figure S 36. Volumetric curve of the dehydrocoupling of $H_3B{\cdot}NMeH_2$ with complex **1**.

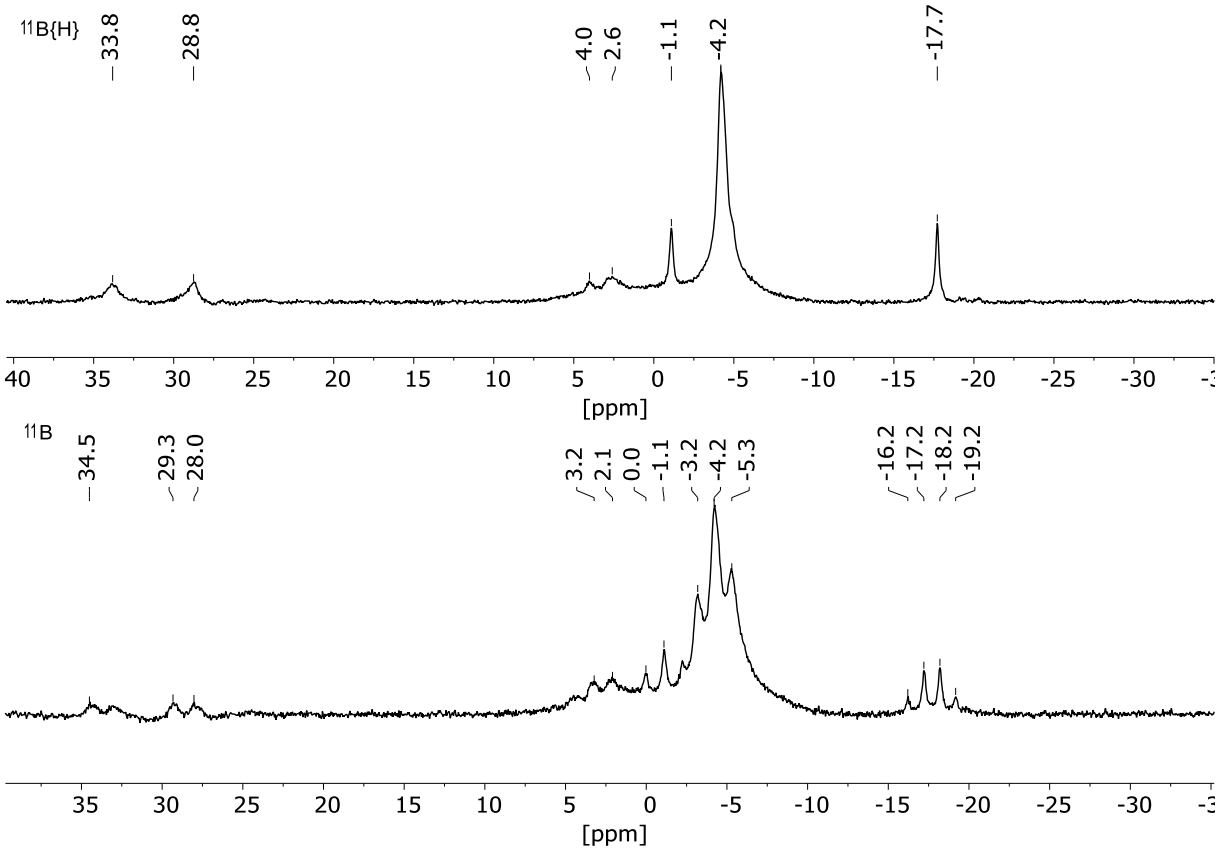

Figure S 37. $^{11}B\{^1H\}$ and ^{11}B NMR spectra (96 MHz, THF-d_8) of dehydrocoupling of $H_3B{\cdot}NMeH_2$ with complex **1**. Conditions: T = 25°C, THF, 1 mol% catalyst.

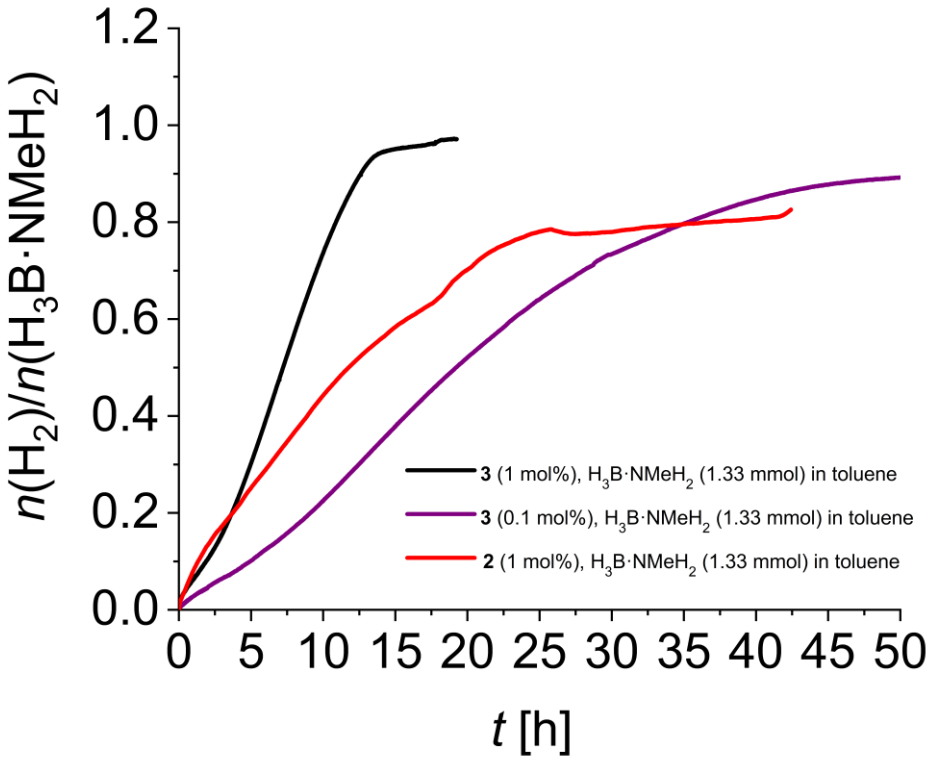

Figure S 38. Volumetric curves of the dehydrocoupling of $H_3B{\cdot}NMeH_2$ with complex **2** and **3**.

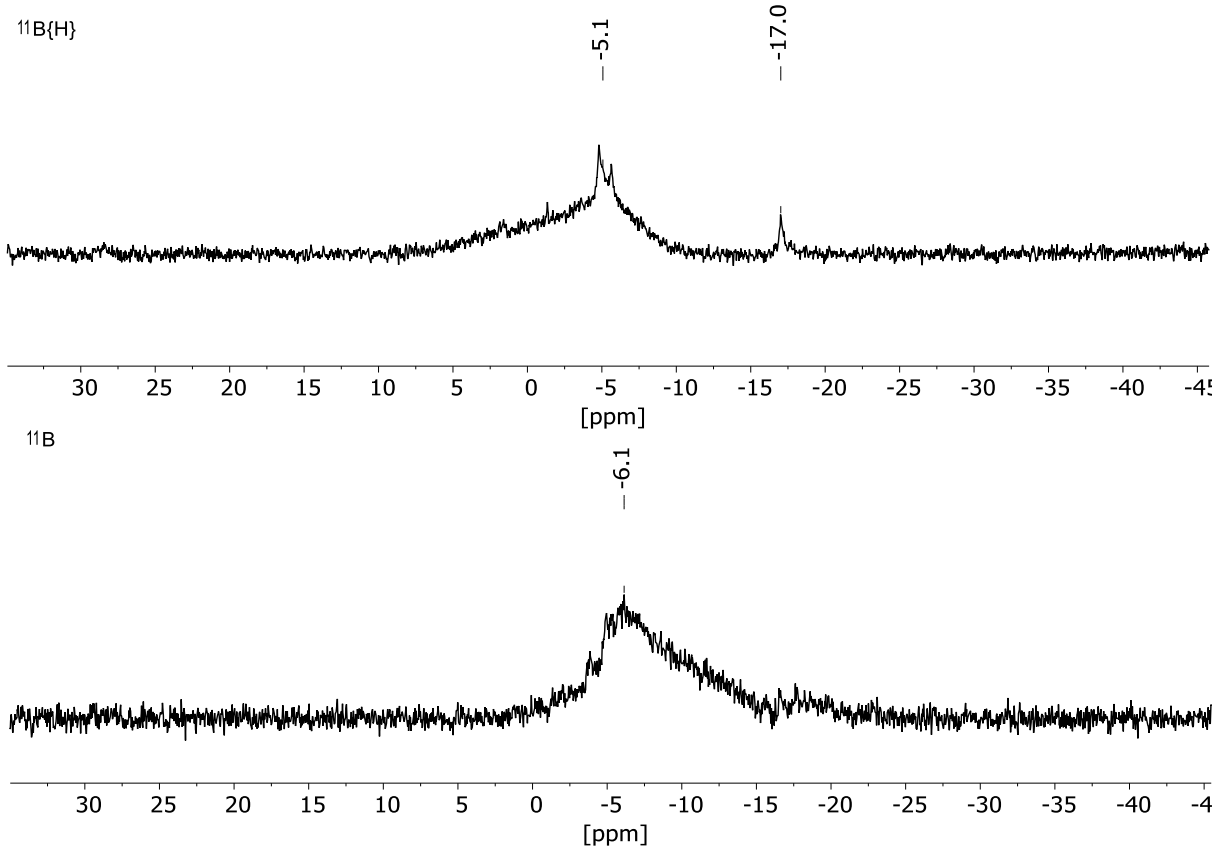

Figure S 39. $^{11}B\{^1H\}$ and ^{11}B NMR spectra (96 MHz, toluene-d_8) of dehydrocoupling of $H_3B{\cdot}NMeH_2$ with complex **3**. Conditions: T = 25°C, toluene, 1 mol% catalyst.

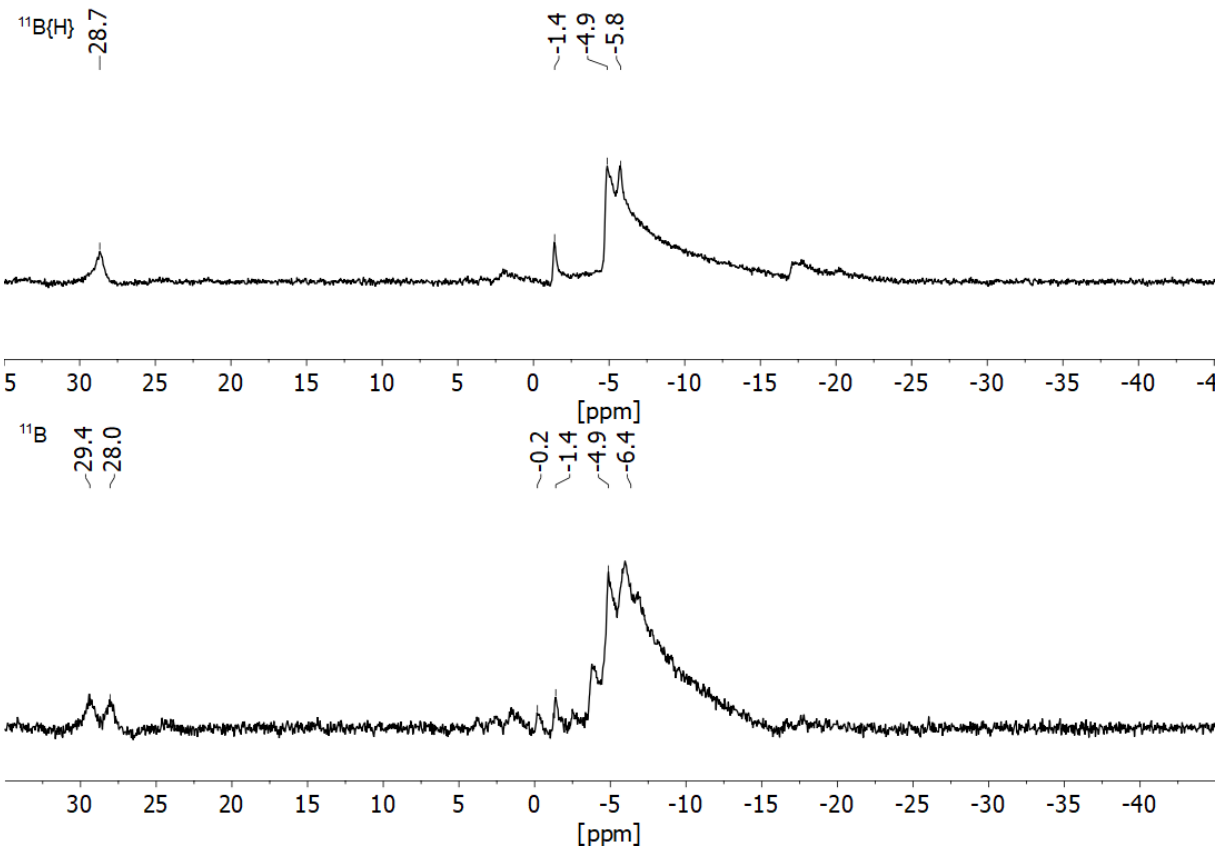

Figure S 40. $^{11}B\{^1H\}$ and ^{11}B NMR spectra (96 MHz, toluene-d_8) of dehydrocoupling of $H_3B{\cdot}NMeH_2$ with complex **2**. Conditions: T = 25°C, toluene, 1 mol% catalyst.

4.4 Reactivity test of 2 for the dehydrocoupling of $H_3B{\cdot}NMeH_2$

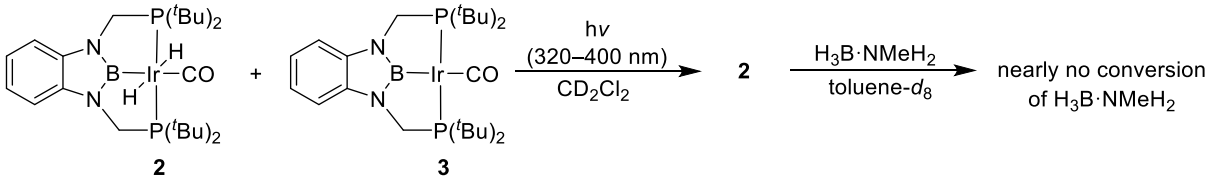

A mixture of complexes **2** and **3** (90:10) in CD_2Cl_2 was irradiated at 320−400 nm in a Young-NMR tube for 20 minutes. The corresponding $^{31}P\{^1H\}$ NMR spectra confirmed the photo-cleavage of complex **3** (Figure S 41) in solution. Afterwards, the solvent was removed in vacuum and toluene-d_8 (0.6 mL) was added, followed by the addition of $H_3B{\cdot}NMeH_2$ (6.0 mg). The ^{11}B and $^{11}B\{^1H\}$ revealed almost no conversion of the substrate after 12 hours (Figure S 42).

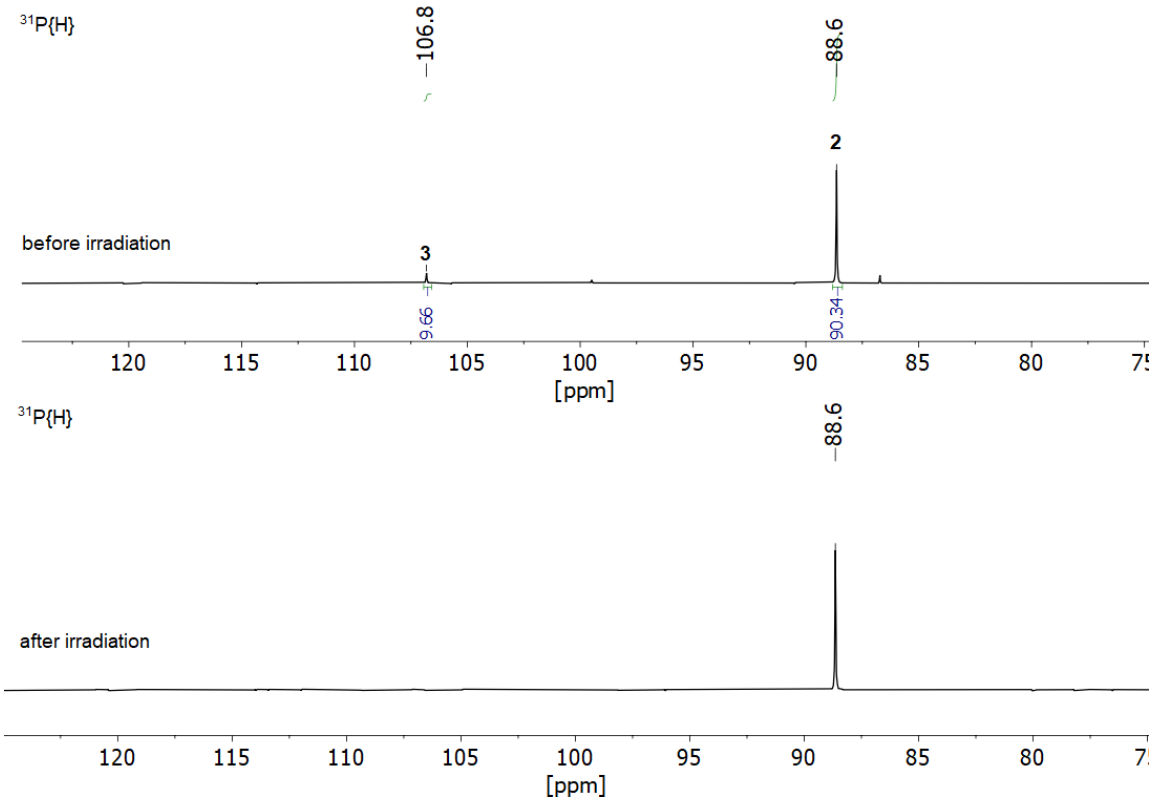

Figure S 41. $^{31}P\{^{1}H\}$ NMR spectra (CD_2Cl_2, 122 MHz, 298 K) of a mixture of complexes **2** and **3**. Top: before irradiation (λ = 320−400 nm). Bottom: after irradiation (t_{total} = 20 min).

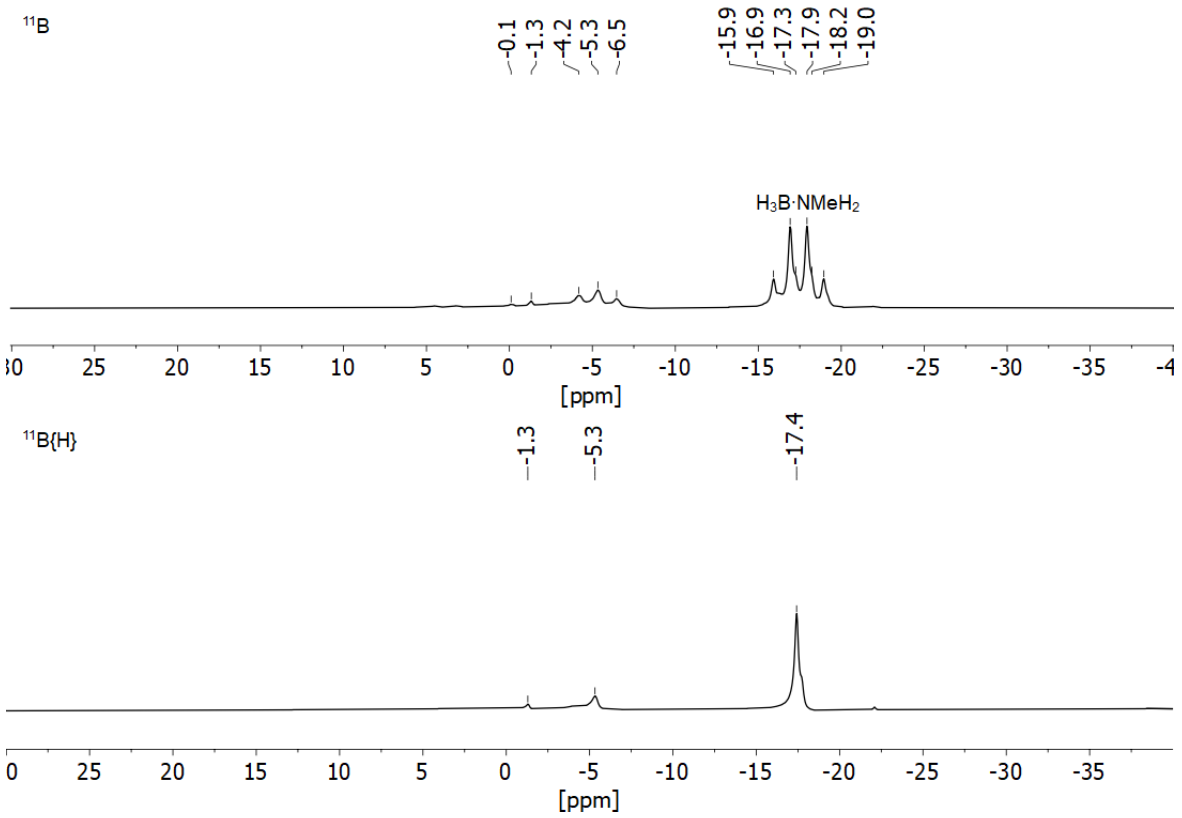

Figure S 42. ^{11}B and $^{11}B\{^{1}H\}$ NMR spectra (96 MHz, toluene-d_8) of dehydrocoupling of $H_3B{\cdot}NMeH_2$ with complex **2** after photocleavage of **3**.

4.5 Dehydrocoupling of $H_3B{\cdot}NH_3$

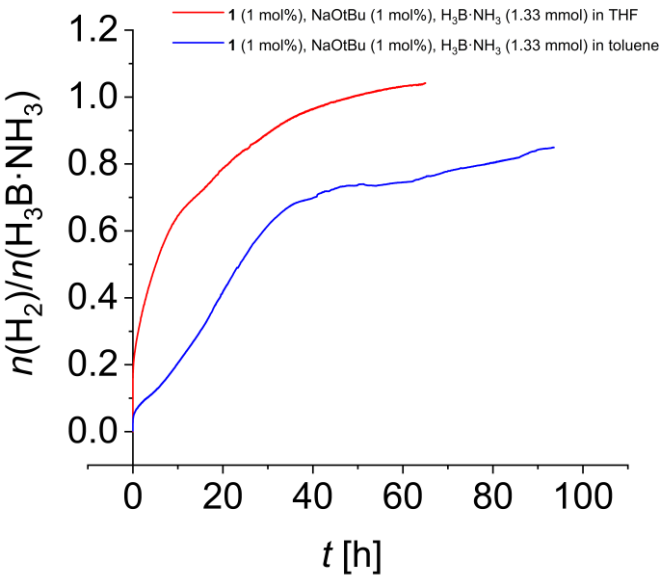

Figure S 43. Volumetric curves of the dehydrocoupling of $H_3B{\cdot}NH_3$ with complex **1**.

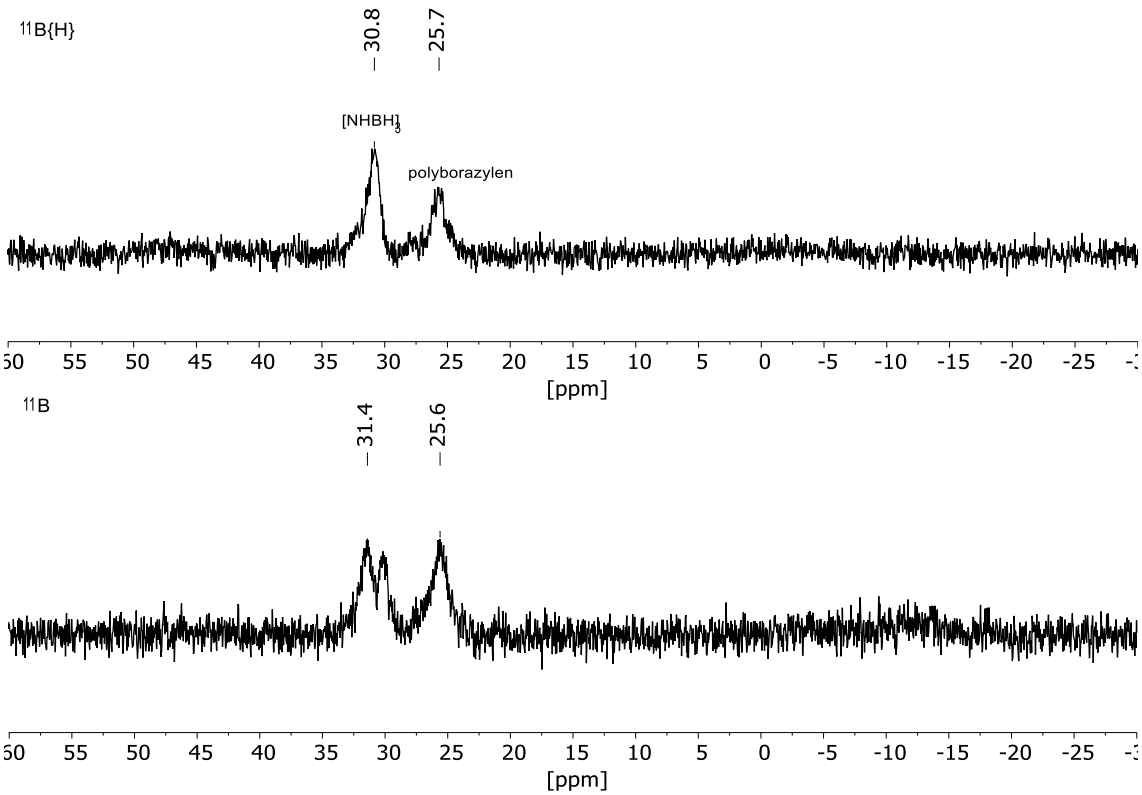

Figure S 44. $^{11}B\{^1H\}$ and ^{11}B NMR spectra (96 MHz, THF-d_8) of dehydrocoupling of $H_3B{\cdot}NH_3$ with complex **1**. Conditions: T = 25°C, THF, 1 mol% catalyst.

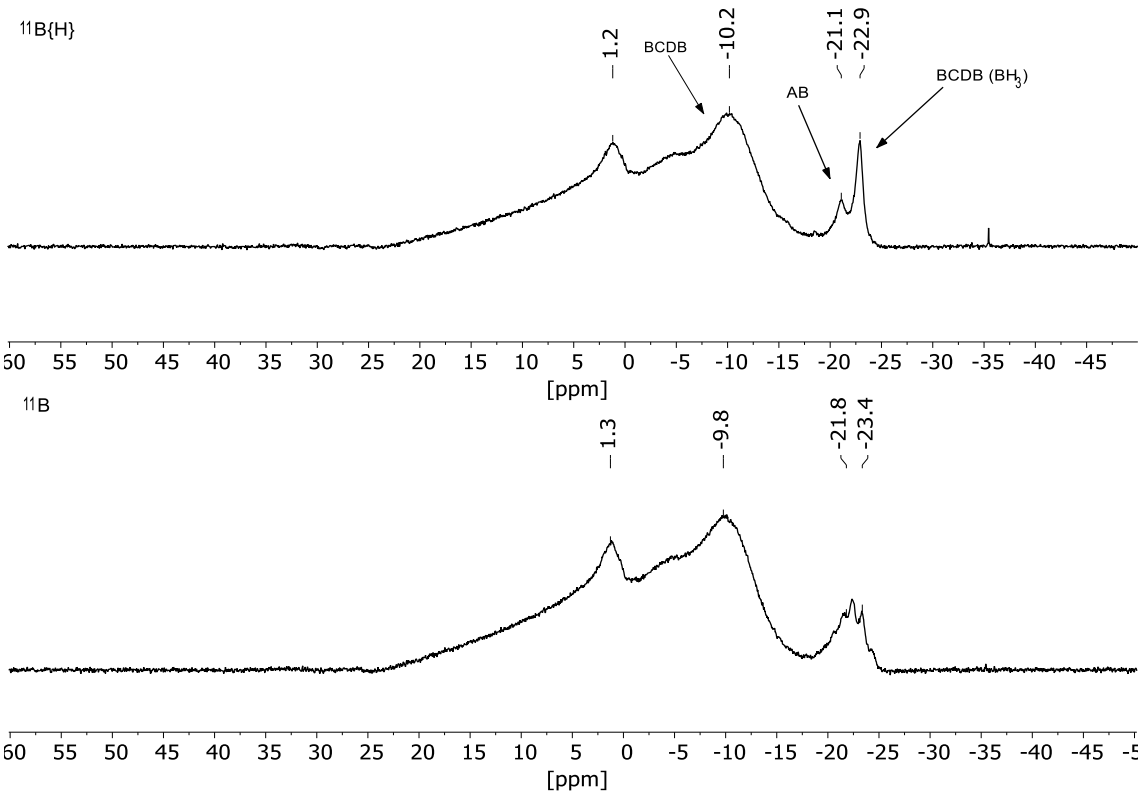

Figure S 45. $^{11}B\{^{1}H\}$ and ^{11}B NMR spectrum (96 MHz, DMSO-d_6) of dehydrocoupling of $H_3B{\cdot}NH_3$ with complex **1** after work up. Conditions: T = 25°C, THF, 1 mol% catalyst.

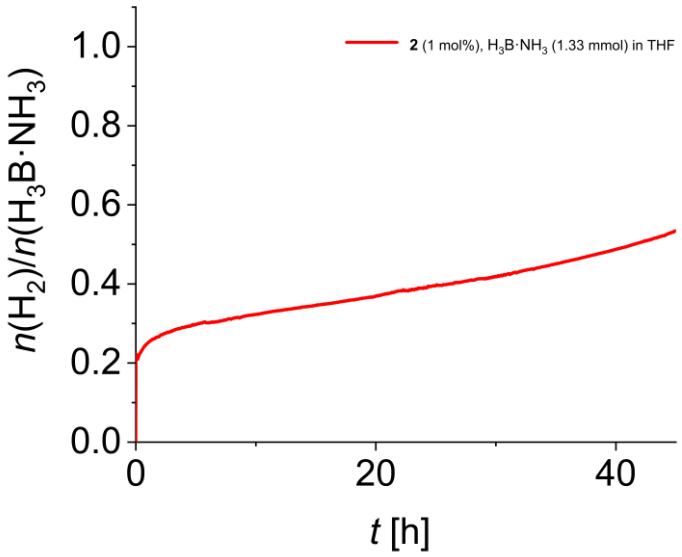

Figure S 46. Volumetric curve of the dehydrocoupling of $H_3B{\cdot}NH_3$ with complex **2**.

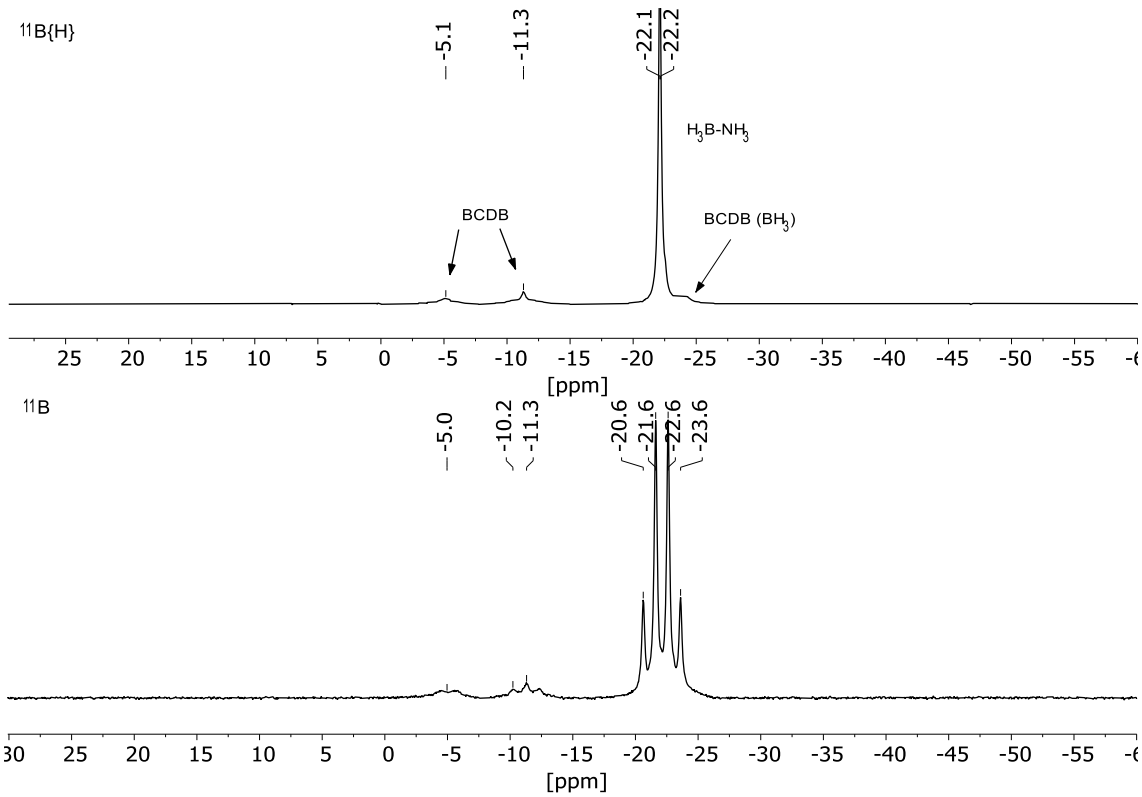

Figure S 47. $^{11}B\{^{1}H\}$ and ^{11}B NMR spectrum (96 MHz, THF-d_8) of dehydrocoupling of $H_3B{\cdot}NH_3$ with complex **2**. Conditions: T = 25°C, THF, 1 mol% catalyst.

5 Computational Details

Computations were carried out using Gaussian16[9]. In our calculations, we have used the real-size molecules. Calculations were carried out using hybrid functional density functional method B3LYP[10-15] in combination with basis set def2tzvp[16] and the empirical dispersion correction GD3BJ[17, 18]. All geometries were confirmed to be local minima or first order saddle points (for transition states, TS) on the potential energy surface by harmonic vibration frequency calculations on the same level of theory. Transition states were proofed to be correct by intrinsic reaction coordinate scans in both directions. For the visualisation of the charge density difference between the ground state and selected excited states as well as for QT-AIM[19, 20] and Laplacians-Plot Analysis we used MultiWfn 3.6 employing Gaussian16 formatted checkpoint files.[21] For the visualisation of 3D-quantum chemical results we used GaussView6.1.1[22] and Avogadro[23, 24]. In addition to the electronic supporting information we provide a multi-structure xyz-file including all calculated molecules. For a better understanding and a more intuitive view of the calculated 3D structures, we strongly recommend using this file e.g. with the free program MERCURY.[25]

Please note that all computations were carried out for single, isolated molecules in the gas phase, if not otherwise noted (ideal gas approximation). There may well be significant differences between gas phase and condensed phase.

Table S 4. Summary of thermodynamic data of all calculated compounds.

Comp. label	File-Name	Nimag	HF	ZPE [kcal/mol]	H_{tot} [a.u.]	G_{tot} [a.u.]	Method	Basisset	Cacl
2	t^{Bu}PBPIr(H)$_2$CO	0	-1977.966957	422.412660	-1977.254478	-1977.359510	B3LYP/GD3BJ	def2tzvp	opt/freq
	t^{Bu}PBPIr(H)$_2$	0	-1864.540911	416.184820	-1863.840140	-1863.942443	B3LYP/GD3BJ	def2tzvp	opt/freq
3	t^{Bu}PBPIr(CO)	0	-1976.761654	411.473630	-1976.066455	-1976.173802	B3LYP/GD3BJ	def2tzvp	opt/freq
int1	PBPIrH4_iso2xray_b3lyp_opt_freq_tzvp.out	0	-1865.7421097	427.42039	-1865.023388	-1865.124840	B3LYP/GD3BJ	def2tzvp	opt/freq
int3	PBPIrH4_iso1_b3lyp_opt_freq_tzvp.out	0	-1865.7405711	426.46881	-1865.022835	-1865.124493	B3LYP/GD3BJ	def2tzvp	opt/freq
int1	PBPIrH4_iso2_b3lyp_opt_freq_tzvp.out	0	-1865.7421097	427.42390	-1865.023383	-1865.124833	B3LYP/GD3BJ	def2tzvp	opt/freq
int1_1	PBPIrH4_iso2_2_opt_freq_tzvp.out	0	-1865.7421097	427.42396	-1865.023383	-1865.124834	B3LYP/GD3BJ	def2tzvp	opt/freq
int2	PBPIrH4_iso3_b3lyp_opt_freq_tzvp.out	0	-1865.7297392	426.63010	-1865.011766	-1865.113813	B3LYP/GD3BJ	def2tzvp	opt/freq
	PBPIrH4_iso3_2_b3lyp_opt_freq_tzvp.out	0	-1865.7421097	427.42203	-1865.023384	-1865.124843	B3LYP/GD3BJ	def2tzvp	opt/freq
TS5	PBPIrH4_TS1_b3lyp_opt_freq_tzvp-1.out	1	-1865.7385889	426.21145	-1865.021703	-1865.122481	B3LYP/GD3BJ	def2tzvp	opt/freq
TS4	PBPIrH4_TS2_b3lyp_opt_freq_tzvp.out	1	-1865.7338617	425.32428	-1865.018344	-1865.119321	B3LYP/GD3BJ	def2tzvp	opt/freq
	PBPIrH4_TS3_b3lyp_opt_freq_tzvp.out	1	-1865.7288988	425.52371	-1865.012970	-1865.114261	B3LYP/GD3BJ	def2tzvp	opt/freq
TS2	PBPIrH4_TS3_2_b3lyp_opt_freq_tzvp.out	1	-1865.7302877	425.51275	-1865.014429	-1865.115628	B3LYP/GD3BJ	def2tzvp	opt/freq
TS1	PBPIrH4_TS4_b3lyp_opt_freq_tzvp2.out	1	-1865.7401797	426.23189	-1865.023487	-1865.124352	B3LYP/GD3BJ	def2tzvp	opt/freq
TS3	PBPIrH4_TS5_b3lyp_opt_freq_tzvp.out	1	-1865.7219982	426.69645	-1865.00422	-1865.105651	B3LYP/GD3BJ	def2tzvp	opt/freq
TS5_Cs	PBPIrH4_TS1_Cs_b3lyp_opt_freq_tzvp.out	1	-1865.7384428	426.11433	-1865.021651	-1865.122919	B3LYP/GD3BJ	def2tzvp	opt/freq

5.1 IR spectra of [(^{tBu}PBP)Ir(H)$_2$(CO)] (2)

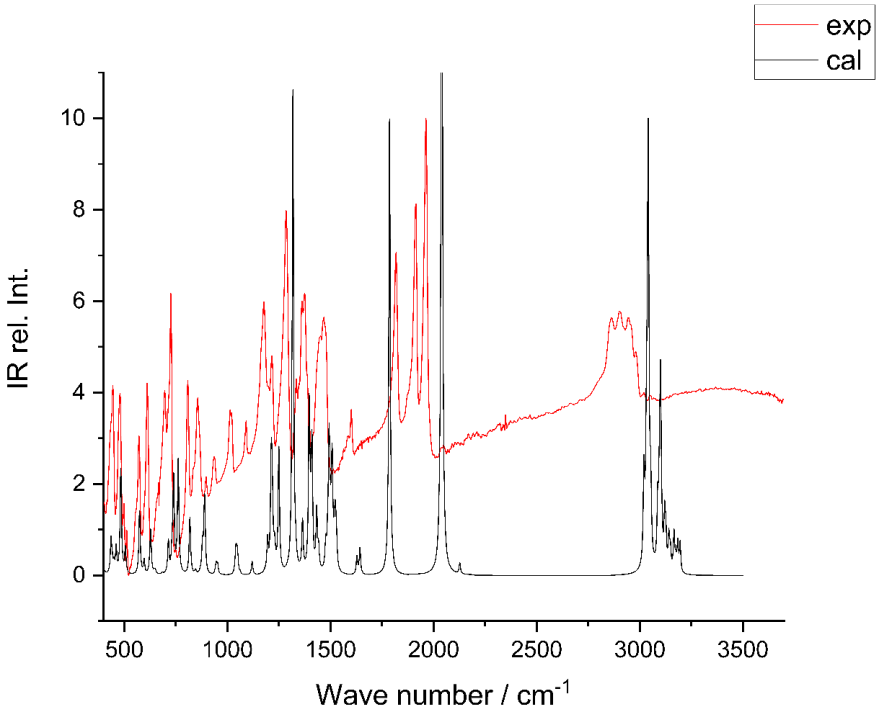

Figure S 48. Calculated (black, B3LYP/GD3BJ/def2tzvp) and experimental (red) IR spectra of complex **2**.

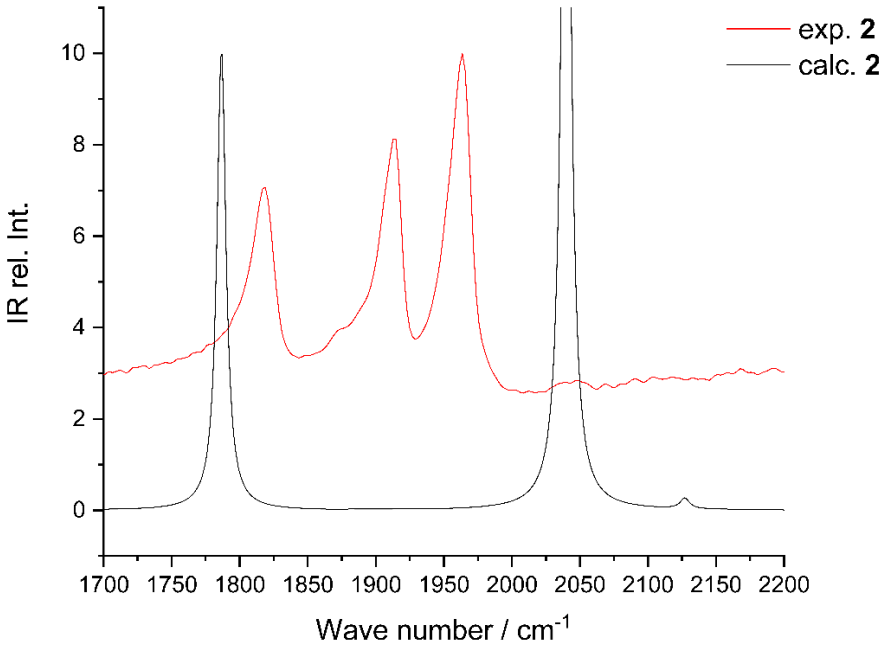

Figure S 49. Calculated (black, B3LYP/GD3BJ/def2tzvp) and experimental (red) IR spectra of complex **2**. Experimental: $\tilde{\nu}$ 2037.0 cm^{-1} (Ir−H), 1963.6 cm^{-1} (Ir−CO), 1818.8 cm^{-1} (Ir−H). Calculated: $\tilde{\nu}_{cal}$ 2127 cm^{-1} (Ir−H), $\tilde{\nu}_{cal}$ 2040 cm^{-1} (Ir−CO), $\tilde{\nu}_{cal}$ 1787 cm^{-1} (Ir−H); Note: $\tilde{\nu}$ 1912.6 cm^{-1} (Ir−CO) of **3**.

5.2 Calculated IR spectra of [($^{t\text{Bu}}$PBP)Ir(CO)] (3)

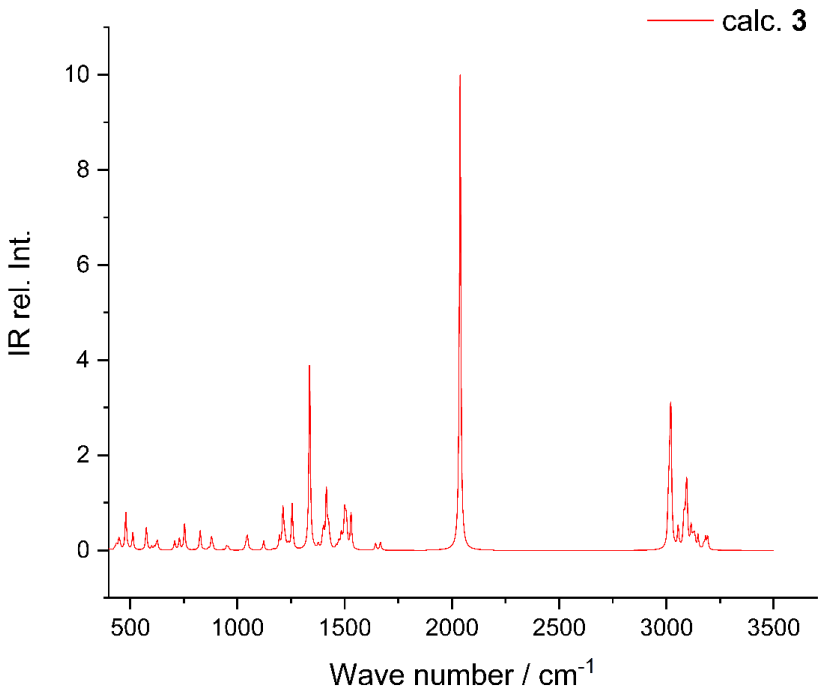

Figure S 50. Calculated (B3LYP/GD3BJ/def2tzvp) IR spectra of complex **3**, $\tilde{\nu}_{calc.}$ 2001 cm^{-1} (Ir−CO).

5.3 Calculated UV/VIS spectra of [(^{tBu}PBP)Ir(H)$_2$(CO)] (2)

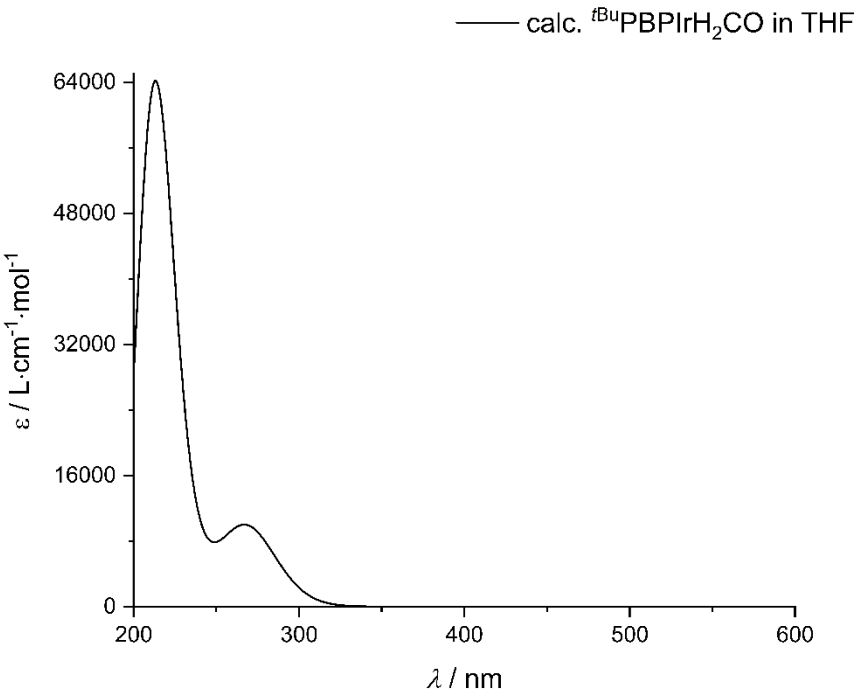

Figure S 51. Calculated (B3LYP/GD3BJ/def2tzvp) UV/VIS spectra of complex **2** with solvent correction in THF.

5.4 Calculated UV/VIS spectra of ^{tBu}PBPIr(CO) (3)

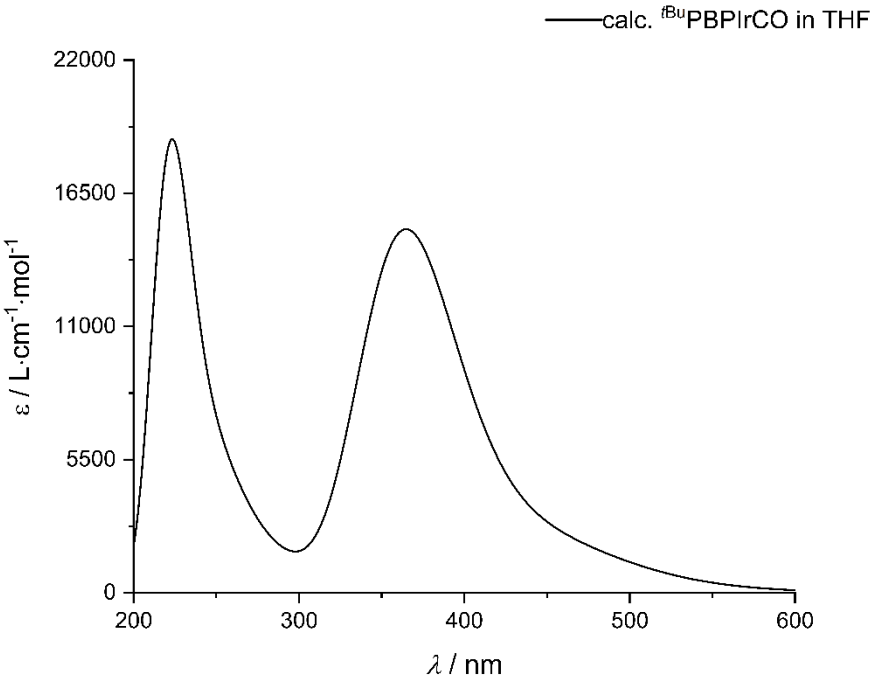

Figure S 52. Calculated (B3LYP/GD3BJ/def2tzvp) UV/VIS spectra of complex **3** with solvent correction in THF.

Excitation energies and oscillator strengths:

Excited State 3: Singlet-A 3.4118 eV 363.40 nm f=0.2904 <S**2>=0.000

129 -> 135 0.10197

133 -> 135 0.68617

Excited State 30: Singlet-A 5.6289 eV 220.26 nm f=0.3088 <S**2>=0.000

129 -> 136 0.41690

130 -> 137 -0.34891

131 -> 137 0.20435

131 -> 138 0.19383

133 -> 136 0.16445

133 -> 141 -0.16388

133 -> 146 -0.11401

Table S 5. Orbital contour plot of the exited state 3 (363.4 nm) of $^{t\text{Bu}}$PBPIr(CO).

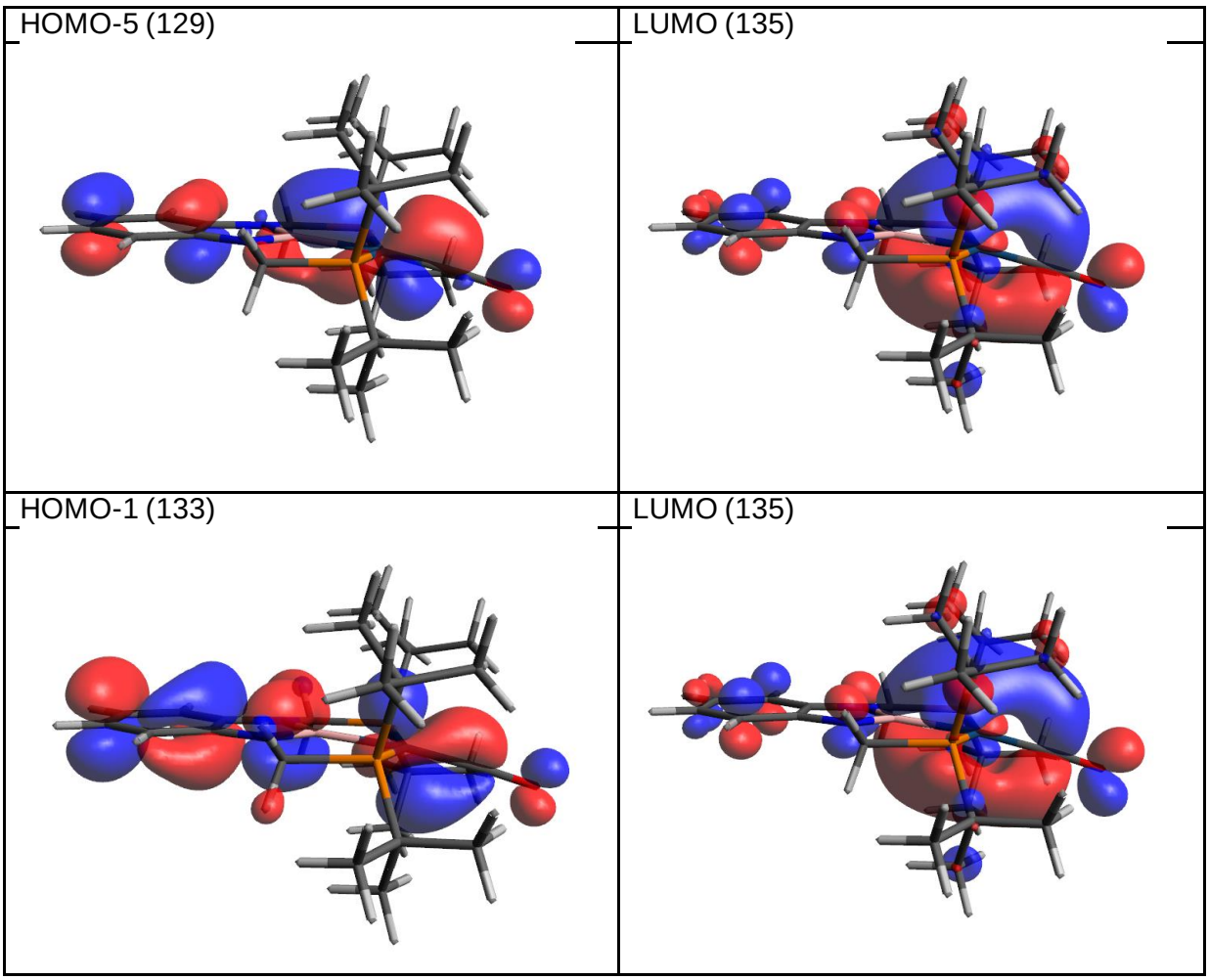

5.5 Charge density difference

Table S 6. Charge density contour plot of complex **3** at the exited state 3 (363.4 nm).

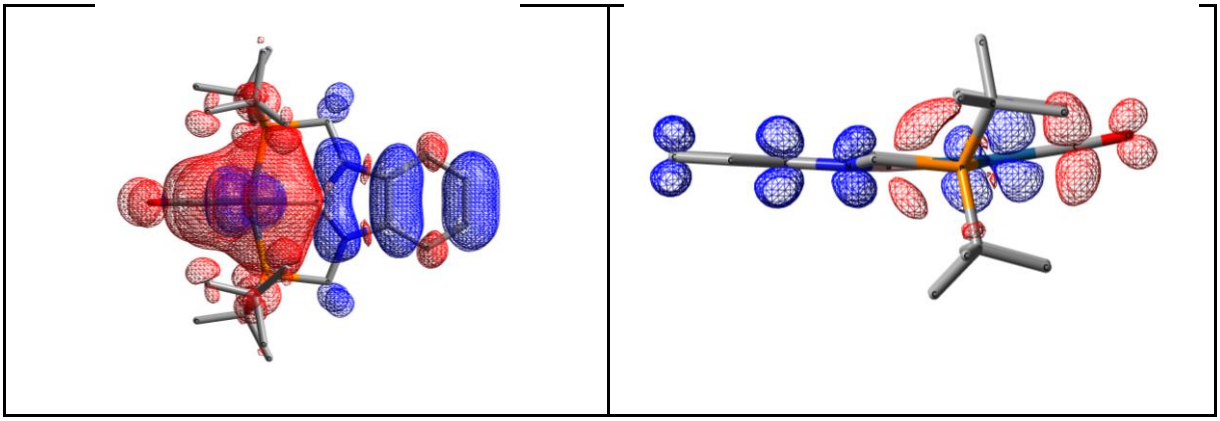

5.6 Theoretical investigation of [(^{tBu}PBP)Ir(H)$_4$] (4)

In this chapter, we summarise the results of our DFT calculations performed at the B3LYP/GD3BJ/def2tzvp level of theory in terms of the energy difference of all isomeric structures of tetrahydride complex **4** considered. Previous studies showed that the potential energy surface of such iridium tetrahydride and/or dihydrogen/dihydride complexes is very low. Noteworthy to mention that Goldman, Krogh-Jespersen *et. al.*[26] revealed a slight shift of the energy surface of [(POCOP)Ir(H)$_4$] pincer complex when considering a solvent correction but only small differences in energy between the considered isomers were reported. This agrees well with our calculations. It should be mentioned that these small differences are below the error of the calculations and should therefore be discussed with caution. A detailed analysis of the data can be found in the manuscript.

Table S 7. Summary of calculated thermodynamic data for the *trans*-pathway of the tetrahydride dihydrogen/dihydride exchange of complex **4.**

Comp. Label	Calc. label	Δ_RH [kJ/mol]	Δ_RG [kJ/mol]	Δ_RH [kcal/mol]	Δ_RG [kcal/mol]
int1_2	PBPIrH4_iso2_2_opt_freq_tzvp.out	0.0	0.0	0.0	0.0
TS1	PBPIrH4_TS4_b3lyp_opt_freq_tzvp.out	-0.3	1.3	-0.1	0.3
int1	PBPIrH4_iso2xray_b3lyp_opt_freq_tzvp.out	0.0	0.0	0.0	0.0
TS4	PBPIrH4_TS2_b3lyp_opt_freq_tzvp.out	13.2	14.5	3.2	3.5
int3	PBPIrH4_iso1_b3lyp_opt_freq_tzvp.out	1.5	0.9	0.3	0.2
TS5	PBPIrH4_TS1_Cs_b3lyp_opt_freq_tzvp.out	4.4	6.2	1.1	1.5
int3_2	PBPIrH4_iso1_b3lyp_opt_freq_tzvp.out	1.5	0.9	0.3	0.2

Table S 8. Summary of calculated thermodynamic data for the *cis*-pathway of the tetrahydride dihydrogen/dihydride exchange of complex **4.**

Comp. Label	Calc. label	Δ_RH [kJ/mol]	Δ_RG [kJ/mol]	Δ_RH [kcal/mol]	Δ_RG [kcal/mol]
int1	PBPIrH4_iso2xray_b3lyp_opt_freq_tzvp.out	0.0	0.0	0.0	0.0
TS2	PBPIrH4_TS3_2_b3lyp_opt_freq_tzvp.out	23.5	24.2	5.6	5.8
int2	PBPIrH4_iso3_b3lyp_opt_freq_tzvp.out	30.5	29.0	7.3	6.9
TS3	PBPIrH4_TS5_b3lyp_opt_freq_tzvp.out	50.3	50.4	12.0	12.0
int2_2	PBPIrH4_iso3_b3lyp_opt_freq_tzvp.out	30.5	29.0	7.3	6.9

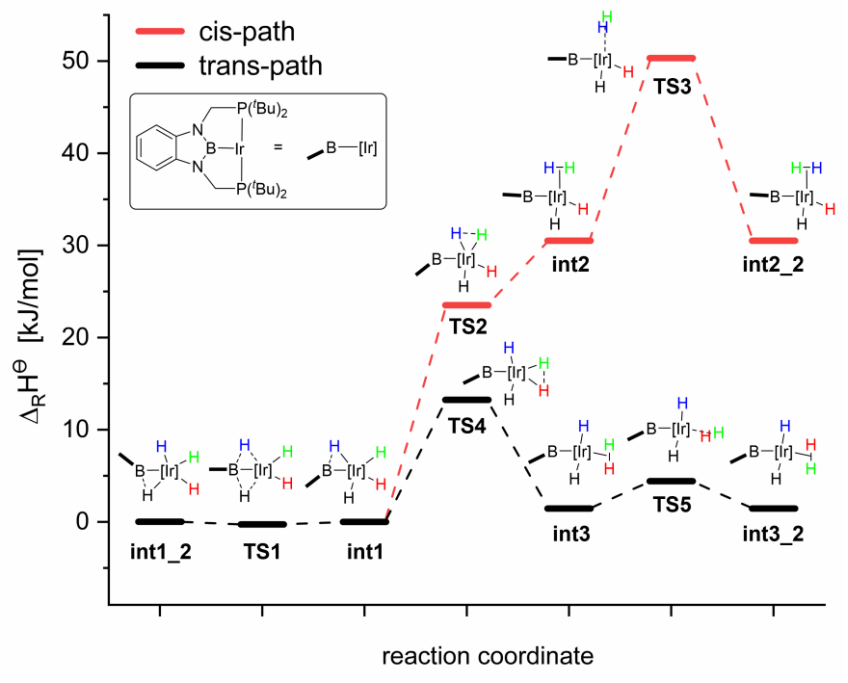

Figure S 53. Plot of the calculated reaction enthalpies for the iridium polyhydride system **4** (B3LYP/GD3BJ/def2tzvp).

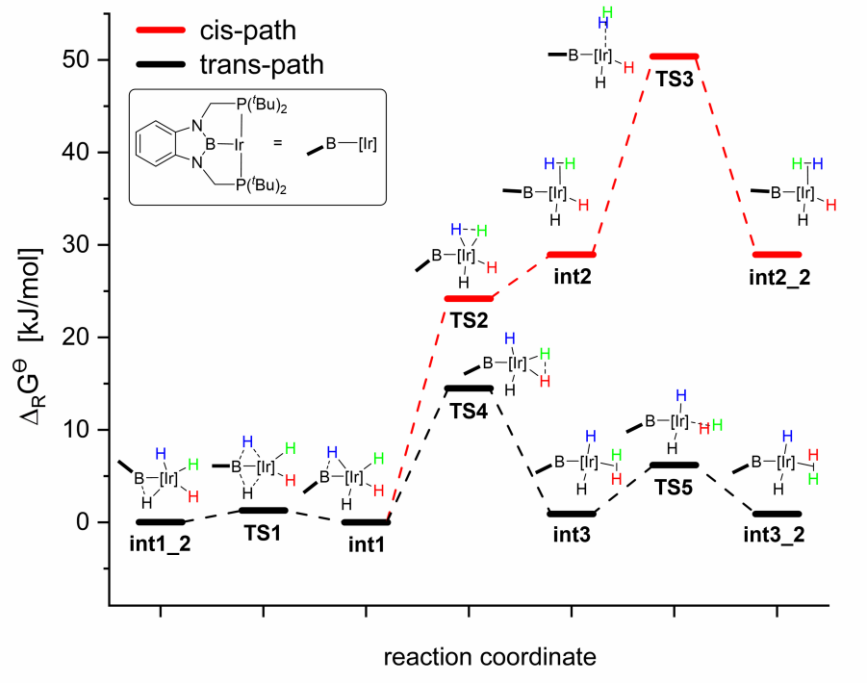

Figure S 54. Plot of the calculated Gibbs free reaction energies for the iridium polyhydride system **4** (B3LYP/GD3BJ/def2tzvp).

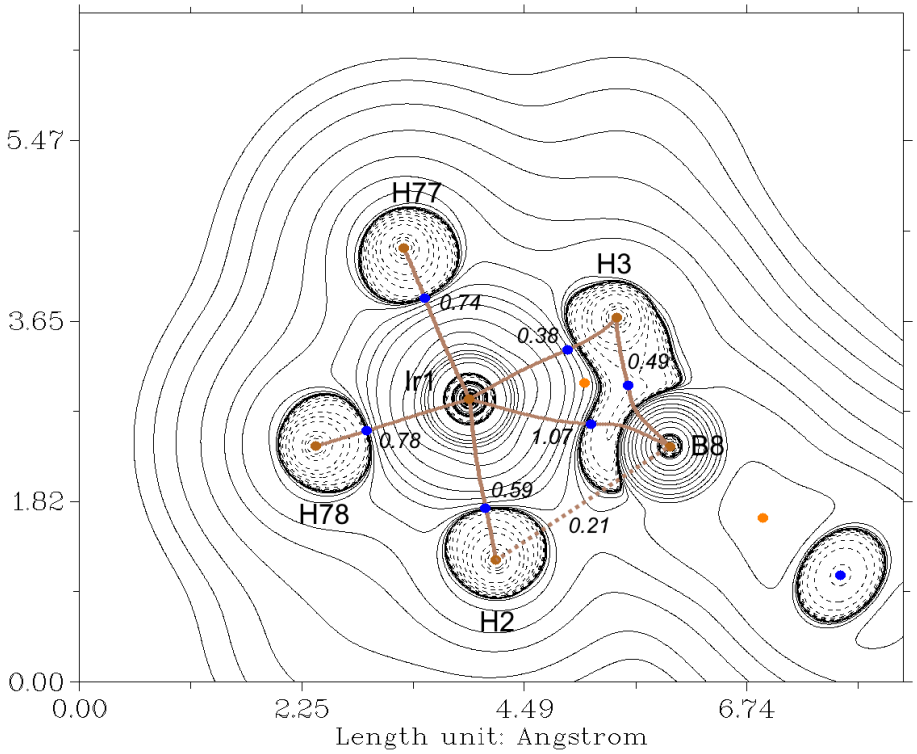

Figure S 55. Contour plot of the Laplacian of the electron density $\nabla^2 r$ of Ir complex **4** in the B-Ir-H plane of **int1** structure. Dashed lines indicate negative (local charge concentration), solid lines indicate positive values (local charge depletion). The Laplacian plot is overlaid with the molecular graph from QT-AIM analysis and wiberg bond indices (italic small numbers). Brown lines indicate bond paths, blue dots correspond to bond critical points, dashed brown lines are hypothetical bond path which were drawn manually in this graph. Density from B3LYP/GD3BJ/def2tzvp calculation.

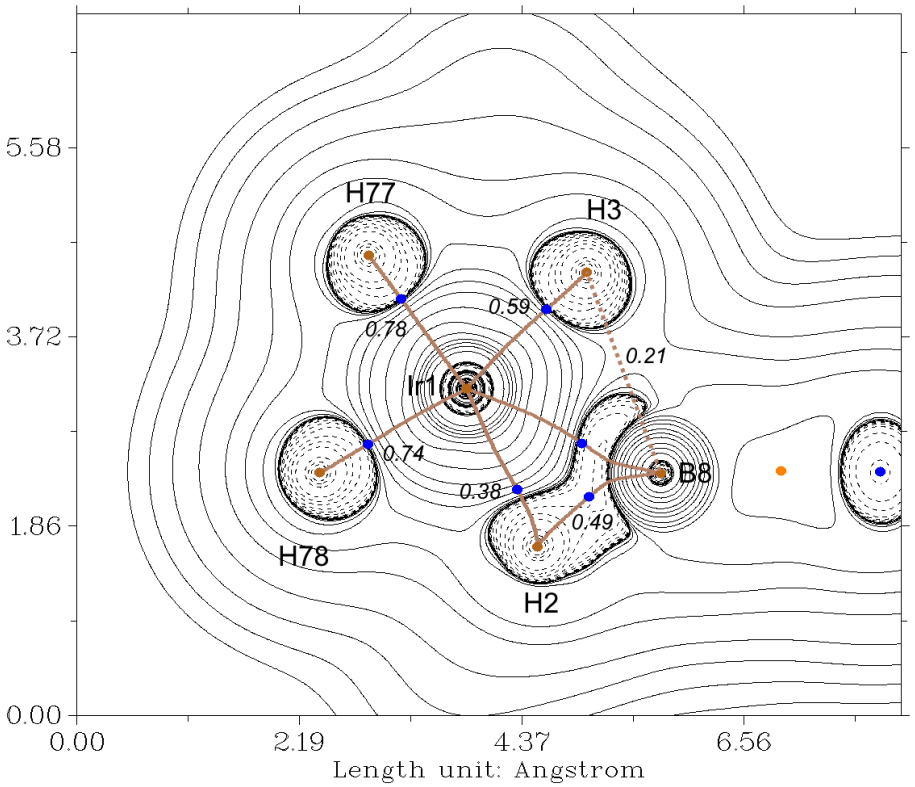

Figure S 56. Contour plot of the Laplacian of the electron density $\nabla^2 r$ of Ir complex **4** in the B-Ir-H plane of **int1_2** structure. Dashed lines indicate negative (local charge concentration), solid lines indicate positive values (local charge depletion). The Laplacian plot is overlaid with the molecular graph from QT-AIM analysis and wiberg bond indices (italic small numbers). Brown lines indicate bond paths, blue dots correspond to bond critical points, dashed brown lines are hypothetical bond path which were drawn manually in this graph. Density from B3LYP/GD3BJ/def2tzvp calculation.

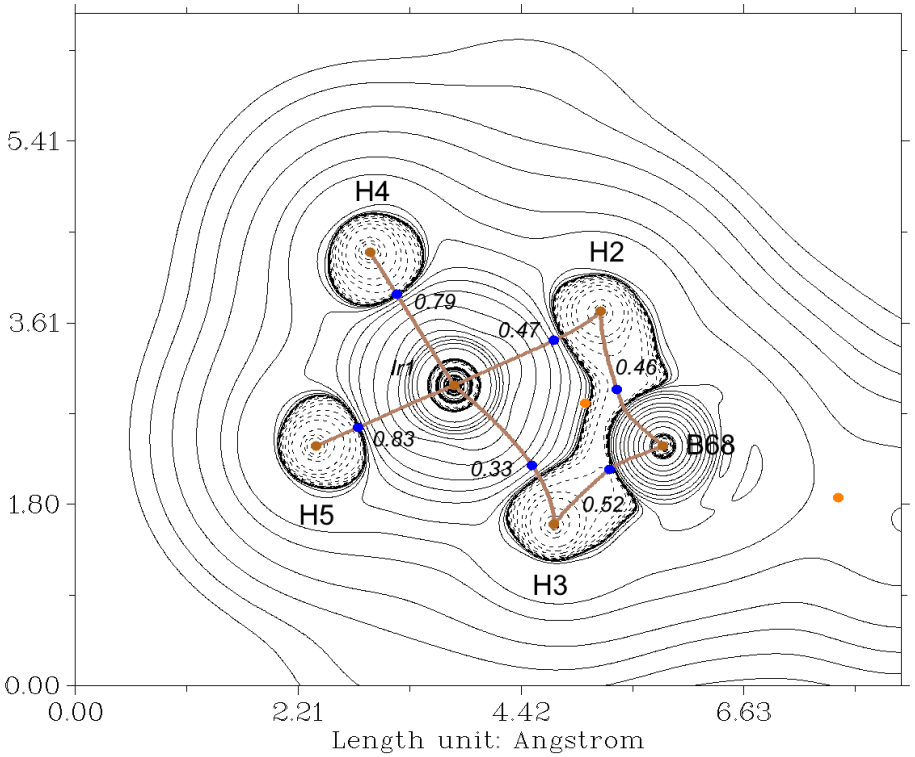

Figure S 57. Contour plot of the Laplacian of the electron density $\nabla^2 r$ of Ir complex **A** in the B-Ir-H plane. Dashed lines indicate negative (local charge concentration), solid lines indicate positive values (local charge depletion). The Laplacian plot is overlaid with the molecular graph from QT-AIM analysis and wiberg bond indices (italic small numbers). Brown lines indicate bond paths, blue dots correspond to bond critical points. Density from B3LYP/GD3BJ/def2tzvp calculation.

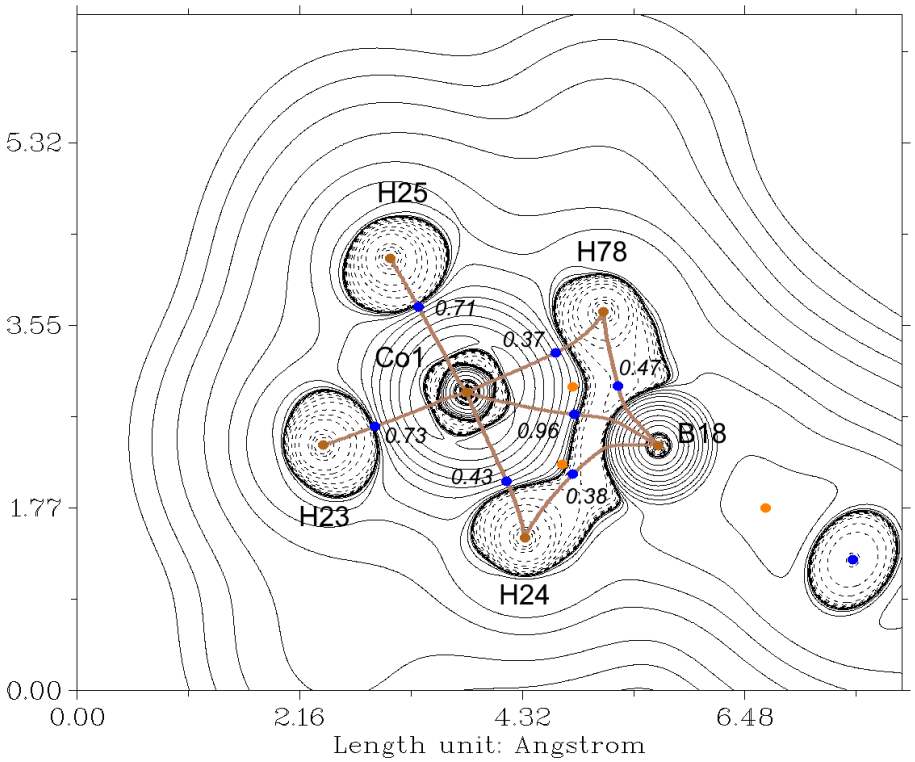

Figure S 58. Contour plot of the Laplacian of the electron density $\nabla^2 r$ of Ir complex **B** in the B-Ir-H plane. Dashed lines indicate negative (local charge concentration), solid lines indicate positive values (local charge depletion). The Laplacian plot is overlaid with the molecular graph from QT-AIM analysis and wiberg bond indices (italic small numbers). Brown lines indicate bond paths, blue dots correspond to bond critical points. Density from B3LYP/GD3BJ/def2tzvp calculation.

Table S 9: Summary of Natural Charge Analysis from NBO6.0[27-30] calculations of the literature known complex **B** and the here described complex **4**.

	Atom	Number	Nat Charge		Atom	Number	Nat Charge
MH_4 unit	Co	1	-0.36171		Ir	1	-0.29141
	H	23	-0.07121		H bridge	75	0.03638
	H bridge	24	0.0082		H	76	-0.09196
	H	25	-0.12761		H	77	-0.08713
	H bridge	78	0.0393		H	78	-0.22703
		Sum	-0.51303			Sum	-0.66115
2 x $CH_2Pt\,Bu_2$	P	2	1.17855		P	2	1.21259
	P	3	1.17936		P	3	1.21272
	C	6	-0.50462		C	5	-0.33039
	H	7	0.20426		C	6	-0.60306
	H	8	0.20161		H	7	0.22677
	C	9	-0.50444		H	8	0.19745
	H	10	0.20161		H	9	0.20631
	H	11	0.20419		C	10	-0.60013
	C	26	-0.31054		H	11	0.20143
	C	27	-0.61033		H	12	0.20354
	H	28	0.20432		H	13	0.23351
	H	29	0.2328		C	14	-0.33212
	H	30	0.20381		C	15	-0.60339
	C	31	-0.60753		H	16	0.20588
	H	32	0.20826		H	17	0.2243
	H	33	0.20255		H	18	0.20539
	H	34	0.20668		C	19	-0.60828
	C	35	-0.6097		H	20	0.20017
	H	36	0.20616		H	21	0.24002
	H	37	0.199		H	22	0.20066
	H	38	0.2282		C	23	-0.59924
	C	39	-0.31064		H	24	0.20831
	C	40	-0.60757		H	25	0.19906
	H	41	0.20826		H	26	0.20001
	H	42	0.20673		C	27	-0.52205
	H	43	0.20257		H	28	0.20194
	C	44	-0.61035		H	29	0.20956
	H	45	0.20431		C	42	-0.52204
	H	46	0.20382		H	43	0.20955
	H	47	0.23287		H	44	0.20194
	C	48	-0.60972		C	45	-0.33212
	H	49	0.20618		C	46	-0.59923
	H	50	0.22814		H	47	0.2
	H	51	0.199		H	48	0.19906
	C	52	-0.31027		H	49	0.20831
	C	53	-0.60596		C	50	-0.60339
	H	54	0.20885		H	51	0.20588
	H	55	0.20128		H	52	0.20539
	H	56	0.20178		H	53	0.2243
	C	57	-0.60964		C	54	-0.60827
	H	58	0.2065		H	55	0.20066
	H	59	0.20747		H	56	0.24001
	H	60	0.22399		H	57	0.20016
	C	61	-0.61255		C	58	-0.33038
	H	62	0.20239		C	59	-0.60013
	H	63	0.23682		H	60	0.20142
	H	64	0.20137		H	61	0.2335
	C	65	-0.31066		H	62	0.20353
	C	66	-0.61247		C	63	-0.60185
	H	67	0.20237		H	64	0.2078
	H	68	0.20146		H	65	0.20064
	H	69	0.2367		H	66	0.20609
	C	70	-0.6096		C	67	-0.60306
	H	71	0.20651		H	68	0.19745
	H	72	0.224		H	69	0.22677
	H	73	0.20747		H	70	0.20631
	C	74	-0.60601		C	71	-0.60185
	H	75	0.20888		H	72	0.2061
	H	76	0.20179		H	73	0.20064
	H	77	0.20131		H	74	0.2078
		Sum	1.17158			Sum	1.18195
Benzodiazaboryl unit	N	4	-0.64716		N	4	-0.65544
	N	5	-0.64702		N	30	-0.65545
	B	18	0.4943		B	31	0.63886
	C	12	0.14538		C	32	0.13935
	C	13	-0.26013		C	33	0.13934
	H	14	0.20716		C	34	-0.25253
	C	15	0.14542		H	35	0.20646
	C	16	-0.22648		C	36	-0.22163
	H	17	0.20471		H	37	0.20397
	C	19	-0.22647		C	38	-0.22162
	H	20	0.20472		H	39	0.20397
	C	21	-0.2601		C	40	-0.25253
	H	22	0.20715		H	41	0.20646
		Sum	-0.65852			Sum	-0.52079

6 Literature

1. Y. Segawa, M. Yamashita and K. Nozaki, *J. Am. Chem. Soc.*, 2009, **131**, 9201-9203.
2. G. M. Sheldrick, *Acta Cryst. A*, 2015, **71**, 3-8.
3. G. M. Sheldrick, *SHELXL 97, Program for the Solution of Crystal Structures*, University of Göttingen, 1990.
4. G. M. Sheldrick, *Acta Cryst. C*, 2015, **71**, 3-8.
5. G. Sheldrick, *SADABS Version 2*, University of Göttingen, 2014.
6. G. Sheldrick, *TWINABS*, University of Göttingen, 2008.
7. P. M. N. Đỗ, N. G. Akhmedov, J. L. Petersen, B. S. Dolinar and C. Milsmann, *Chem. Commun.*, 2020, **56**, 5397-5400.
8. T. Beweries, J. Thomas, M. Klahn, A. Schulz, D. Heller and U. Rosenthal, *ChemCatChem*, 2011, **3**, 1865-1868.
9. M. J. Frisch, G. W. Trucks, H. B. Schlegel, G. E. Scuseria, M. A. Robb, J. R. Cheeseman, G. Scalmani, V. Barone, G. A. Petersson, H. Nakatsuji, X. Li, M. Caricato, A. V. Marenich, J. Bloino, B. G. Janesko, R. Gomperts, B. Mennucci, H. P. Hratchian, J. V. Ortiz, A. F. Izmaylov, J. L. Sonnenberg, Williams, F. Ding, F. Lipparini, F. Egidi, J. Goings, B. Peng, A. Petrone, T. Henderson, D. Ranasinghe, V. G. Zakrzewski, J. Gao, N. Rega, G. Zheng, W. Liang, M. Hada, M. Ehara, K. Toyota, R. Fukuda, J. Hasegawa, M. Ishida, T. Nakajima, Y. Honda, O. Kitao, H. Nakai, T. Vreven, K. Throssell, J. A. Montgomery Jr., J. E. Peralta, F. Ogliaro, M. J. Bearpark, J. J. Heyd, E. N. Brothers, K. N. Kudin, V. N. Staroverov, T. A. Keith, R. Kobayashi, J. Normand, K. Raghavachari, A. P. Rendell, J. C. Burant, S. S. Iyengar, J. Tomasi, M. Cossi, J. M. Millam, M. Klene, C. Adamo, R. Cammi, J. W. Ochterski, R. L. Martin, K. Morokuma, O. Farkas, J. B. Foresman and D. J. Fox, *Journal*, 2016.
10. S. H. Vosko, L. Wilk and M. Nusair, *Can. J. Phys.*, 1980, **58**, 1200-1211.
11. J. P. Perdew, *Phys. Rev. B*, 1986, **33**, 8822-8824.
12. A. D. Becke, *Phys. Rev. A*, 1988, **38**, 3098-3100.
13. A. D. Becke, *J. Chem. Phys.*, 1993, **98**, 5648-5652.
14. C. Lee, W. Yang and R. G. Parr, *Phys. Rev. B*, 1988, **37**, 785-789.
15. B. Miehlich, A. Savin, H. Stoll and H. Preuss, *Chem. Phys. Lett.*, 1989, **157**, 200-206.
16. F. Weigend and R. Ahlrichs, *Phys. Chem. Chem. Phys.*, 2005, **7**, 3297-3305.
17. S. Grimme, J. Antony, S. Ehrlich and H. Krieg, *J. Chem. Phys.*, 2010, **132**, 154104.
18. S. Grimme, S. Ehrlich and L. Goerigk, *J. Comput. Chem.*, 2011, **32**, 1456-1465.
19. R. F. W. Bader, *Chem. Rev.*, 1991, **91**, 893-928.
20. F. Richard and R. Bader, *Atoms in Molecules: A Quantum Theory*, Oxford University Press, 1990.
21. T. Lu and F. Chen, *J. Comput. Chem.*, 2012, **33**, 580-592.
22. D. Roy, T. A. Keith and J. M. Millam, *GaussView, Version 6.1*, Shawnee Mission, KS, 2016.
23. Avogadro, *an open-sourece molecular builder and visualization tool*, Version 1.6, **Retrieved from http://avogadro.cc/**.
24. M. D. Hanwell, D. E. Curtis, D. C. Lonie, T. Vandermeersch, E. Zurek and G. R. Hutchison, *Journal of Cheminformatics*, 2012, **4**, 17.
25. Mercury, **Retrieved from http://www.ccdc.cam.ac.uk/mercury/**.
26. T. J. Hebden, K. I. Goldberg, D. M. Heinekey, X. Zhang, T. J. Emge, A. S. Goldman and K. Krogh-Jespersen, *Inorg. Chem.*, 2010, **49**, 1733-1742.
27. E. D. Glendening, C. R. Landis and F. Weinhold, *J. Comput. Chem.*, 2013, **34**, 1429-1437.
28. F. Weinhold and C. R. Landis, *Valency and Bonding: A Natural Bond Orbital Donor-Acceptor Perspective*, Cambridge University Press, Cambridge, 2005.
29. F. Weinhold and J. E. Carpenter, in *The Structure of Small Molecules and Ions*, eds. R. Naaman and Z. Vager, Springer US, Boston, MA, 1988, DOI: 10.1007/978-1-4684-7424-4_24, pp. 227-236.
30. J. E. Carpenter and F. Weinhold, *J. Mol. Struct.: THEOCHEM*, 1988, **169**, 41-62.